International Journal of Nanomedicine

Dovepress
Taylor & Francis Group

Open Access Full Text Article

ORIGINAL RESEARCH

Diosmin-Capped Silver Nanoparticles Promote Osteogenic Differentiation of Human Periodontal Ligament Stem Cells: Box–Behnken Optimization and in vitro Evaluation

Roxane Abdel Gawad[1], Shymaa Hatem[2], Nehal I Rizk[3], Shereen N Raafat[4,5], Dalia E Ali[6], Riham A El-Shiekh[7], Doaa H Shakshak[8]

[1]Department of Pharmaceutics and Industrial Pharmacy, Faculty of Pharmacy, Ain Shams University, Cairo, Egypt; [2]Department of Pharmaceutics and Pharmaceutical Technology, Faculty of Pharmacy, Future University in Egypt, Cairo, Egypt; [3]Department of Biochemistry, Faculty of Pharmacy and Drug Technology, Egyptian Chinese University, Cairo, Egypt; [4]Department of Pharmacology (Medical Sciences), Faculty of Dentistry, The British University in Egypt, El Sherouk City, Cairo, Egypt; [5]Dental Science Research Group, Health Research Centre of Excellence, The British University in Egypt, El Sherouk City, Cairo, Egypt; [6]Department of Pharmacognosy and Natural Products, Faculty of Pharmacy, Pharos University in Alexandria, Alexandria, Egypt; [7]Pharmacognosy Department, Faculty of Pharmacy, Cairo University, Cairo, Egypt; [8]Department of Pharmaceutics and Pharmaceutical Technology, Faculty of Pharmacy, The British University in Egypt, El-Sherouk City, Cairo, Egypt

Correspondence: Doaa H Shakshak; Shymaa Hatem, Email doaahamdy@pharma.asu.edu.eg; shaimaa.hatem@fue.edu.eg

Aim: Diosmin is a bioactive flavonoid with anti-inflammatory, anti-oxidant, and osteogenic properties; however, its poor water solubility limits its therapeutic use. To overcome this, the study developed Diosmin-loaded silver nanoparticles (AgNPs), leveraging the bone-regenerative potential of silver, as a unique strategy to improve the osteogenic differentiation of periodontal ligament stem cells (PDLSCs).

Methods: The nanoparticles loaded with the extracted Diosmin were prepared using a scalable green reduction method and optimized using the Box–Behnken design (BBD) and response surface methodology. Key factors (silver nitrate concentration, Diosmin concentration, and reaction temperature) were assessed for their effects on the particle size, zeta potential, and polydispersity index. This study also evaluated the effects of Diosmin-loaded AgNPs on the viability and osteogenic differentiation of human PDLSCs. Alizarin Red staining and alkaline phosphatase activity were used to assess osteogenic differentiation. Moreover, real-time quantitative polymerase chain reaction (RT-qPCR) was used to track the expression of osteogenic-associated markers, osteoprotegerin (OPG) and runt-related transcription factor 2 (RUNX2), as well as proinflammatory markers, TNF-α and IL-1β.

Results: The optimized Diosmin-loaded AgNPs identified by the BBD showed high desirability, with particle size of 181.0±8.45 nm using dynamic light scattering technique (DLS) and a negative surface charge of −21.45±1.27 mV, confirmed by transmission electron microscopy (TEM) photomicrographs. Moreover, energy-dispersive X-ray (EDX) analysis showed the preparation of AgNPs through showing their elemental peaks. Stability studies demonstrated that formulations remained stable at 4.0±2.0°C for up to 3 months. The results showed that, in contrast to silver nitrate ($AgNO_3$), Diosmin-loaded AgNPs promoted osteogenic differentiation and modulated the expression of inflammatory markers, indicating a potential role in the regulation of the local inflammatory microenvironment associated with osteogenesis.

Conclusion: Green AgNPs have proven their efficacy as a potential approach for osteogenic differentiation.

Keywords: diosmin, silver nanoparticles, green synthesis, box-behnken design, osteogenic differentiation, periodontal ligament stem cells

Introduction

Critical-sized bone defects, also known as massive bone defects, are bone flaws that cannot heal spontaneously. Malignancy, infection, multiple fractures, severe trauma, and musculoskeletal conditions can result in bone abnormalities. The complex physiological process of bone healing involves numerous cells and cell signaling molecules that

https://doi.org/10.2147/IJN.S618588
Received: 20 April 2026
Accepted: 18 June 2026
Published: 24 June 2026

interact at the fracture site to restore bone tissues. The normal mechanism of bone regeneration is insufficient to replace missing tissue in critical-sized bone defects.[1]

To treat bone loss, allogeneic, autologous, or xenogeneic bone transplantation techniques, as well as synthetic biomaterials, are frequently employed in surgical procedures involving bone grafting. Autologous bone transplantation is the most reliable method for repairing significant bone abnormalities.[2] This procedure involves the transplantation of autologous tissue derived from healthy parts of the body, although its use is constrained by a number of factors, such as the potential need for a large volume of bone, pain involved, potential donor site morbidity, lengthy recovery period, and insufficient vascularization. The limitations of autologous bone transplantation have been addressed by introducing synthetic materials intended for bone grafting. The main expense related to their production hinders the widespread use of these graft materials.[3]

Periodontal ligament stem cells (PDLSCs) are emerging as a valuable source for bone tissue regeneration owing to their strong proliferative ability and intrinsic role in maintaining and remodeling periodontal tissues. Originating from the periodontal ligament, these cells are easily obtained from extracted teeth and exhibit excellent adaptability to in vitro culture conditions.[4] PDLSCs exhibit a natural tendency toward hard tissue formation, which makes them particularly suitable for osteogenic applications in periodontal, alveolar, and craniofacial bone repair. Their capacity to survive, migrate, and participate in tissue regeneration highlights their potential usefulness in regenerative dentistry and bone tissue engineering.[5]

When exposed to osteogenic induction conditions, PDLSCs readily differentiate into osteoblast-like cells, as indicated by enhanced alkaline phosphatase (ALP) activity, deposition of mineralized extracellular matrix, and expression of bone-related genes, such as runt-related transcription factor 2 (RUNX2), collagen type I, and osteocalcin.[6] The osteogenic potential of PDLSCs can be significantly influenced by culture conditions, biomaterial scaffolds, growth factors, and mechanical stimuli that mimic the native bone microenvironment.[7] Additionally, important signaling pathways, such as Wnt/β-catenin and BMP-related pathways, play crucial roles in the regulation of osteogenic differentiation. These characteristics make PDLSCs an attractive and effective cell source for developing advanced strategies for bone regeneration and periodontal tissue engineering.[8]

Nanoparticles exhibit remarkable mechanical properties owing to their nanoscale size and surface-to-volume ratio.[9] Nanoparticles have been thoroughly investigated for their potential use in bone tissue regeneration owing to their distinctive structural characteristics, effective drug delivery capabilities, and advantageous biocompatibility.[10] Among them, AgNPs have attracted considerable attention owing to their unique physicochemical properties and significant potential for various biomedical applications.[11] Their physical, chemical, and biological characteristics distinguish them from their bulk counterparts. They exhibit broad-spectrum antibacterial activities against a variety of microbes. AgNPs also aid in the development of fibrous tissue and help bridge fracture sites.[12] Additionally, increasing the expression of bone morphogenetic proteins (BMPs) promotes osteogenic differentiation.[13] Furthermore, after implantation at the site of infected bone defects, AgNPs significantly reduced the levels of inflammatory biomarkers, such as leukocyte count and C-reactive protein (CRP), improving the repair process of impaired bone tissue.[14] However, their practical applicability is limited by the use of hazardous chemicals in conventional chemical synthesis techniques. Accordingly, green synthesis techniques that employ naturally occurring bioactive compounds provide a more environment-friendly approach, rendering more biocompatible nanoparticles in addition to additional therapeutic functionalities.[15] Although AgNPs possess promising regenerative and antimicrobial properties, their biological effects are highly dependent on factors such as particle size, concentration, ion release, surface characteristics, and exposure duration. At low and controlled doses, AgNPs may enhance osteogenesis and antibacterial activity; however, excessive exposure can induce cytotoxicity, oxidative stress, DNA damage, and inflammatory responses, mainly through ROS generation and silver ion release. Therefore, optimizing AgNPs formulation and dosage is essential to ensure therapeutic efficacy while minimizing adverse cellular effects.[16]

Diosmin, also known as 3′,5,7-trihydroxy-4′-7-rhamnoglucoside, is a flavonoid glycoside with anti-inflammatory, anti-oxidant, and vascular protective properties. Diosmin has been reported to have many pharmacological activities, such as anti-oxidant, anti-inflammatory, antihyperlipidemic, and antihyperglycemic effects.[17] Diosmin can enhance bone formation by upregulating key osteogenic markers such as RUNX2, Wnt signaling components, phosphorylated Akt (p-Akt), osteoprotegerin (OPG), osteocalcin, and BCL2. Simultaneously, it inhibits bone resorption by decreasing the generation of reactive

oxygen species (ROS) and downregulating the expression of receptor activator of nuclear factor κB ligand (RANKL).[18] A strong synergistic framework is established by this green synthesis approach. The lipophilic nature of Diosmin with a partition coefficient (log P) of around 2.05 and poor aqueous solubility (0.019 mg/mL) are intrinsic drawbacks, resulting in low oral bioavailability and inconsistent gastrointestinal absorption. This can be successfully circumvented by using nanoparticle-mediated delivery methods to increase its therapeutic efficacy. Moreover, the high surface-area-to-volume ratio of flavonoids encapsulated into nanocarriers such as AgNPs enhances the effective surface area exposed to the aqueous dissolving medium, improving systemic bioavailability. Simultaneously, the use of a natural polyphenolic ingredient results in AgNPs that are more biocompatible by removing the requirement for hazardous synthetic reducing agents. The polyphenolic structure of Diosmin helped to reduce silver ions (Ag+) from silver nitrate ($AgNO_3$), allowing it to work as a dual weapon, reducing agent, and bioactive molecule in the AgNPs formulation.[19]

The current study aimed to investigate a novel eco-friendly synthesis technique for the fabrication of Diosmin-capped AgNPs, exploiting its dual role as a reducing phytochemical and therapeutic moiety, and to explore the resulting nanoformulation as a promising strategy in osteogenic applications. This investigation represents a pioneering attempt to incorporate Diosmin into AgNPs and evaluate its osteogenic potential in PDLSCs.

Materials and Methods

Plant material of Hyssop (Hyssopus officinalis L., Lamiaceae) was purchased from Haraz Herbal Company (Cairo, Egypt). $AgNO_3$ was obtained from Fisher Scientific (UK). Ethyl alcohol 96%), Dimethyl sulfoxide (DMSO), chloroform, sodium hydroxide, formaldehyde, paraformaldehyde, glacial acetic acid, para-nitrophenylphosphate, alkaline phosphatase buffer, and phosphate-buffered saline components were sourced from the International Company for Supportive Medical Industries (ALAMIA), Egypt. Ultrapure distilled water was acquired from MilliQ Plus (Millipore, Iberica, Spain). DMEM/F12 (Dulbecco's Modified Eagle Medium/F12) Ham medium and Alizarin Red, Oil Red O, and Alcian Blue staining solutions were acquired from Sigma (St. Louis, MO, USA). Antibiotic/antimycotic solution and fetal bovine serum (FBS) were acquired from Gibco BRL (Carlsbad, California, USA).

Isolation and Characterization of Diosmin

Diosmin was isolated according to the procedure reported by Bogucka-Kocka et al,[20] in which chloroform was used as defatting solvent, and the plant material was extracted with 96% ethanol. Based on the solubility of Diosmin in DMSO, it was used to solubilize Diosmin from ethanolic extract. Ten-fold water was then added to recrystallize Diosmin from DMSO. After 48 h, the Diosmin precipitate was filtered and collected for further analyses. The structure was elucidated by ^{1}H-NMR and compared with the literature to confirm the isolation of Diosmin (Supplementary Figure 1).[21]

Box Behnken Design (BBD) Construction

Diosmin-loaded AgNPs components were assessed as critical material attributes (CMA), including AgNO3 concentration (A), Diosmin concentration (B), and reaction temperature (C), at 0.5–5 mM, 0.1–0.5 mg/mL, and 60–90°C, respectively, based on a performed preliminary study (data not shown). In each formulation, Diosmin: $AgNO_3$ volume ratio was maintained at 1:10. The zeta potential (ZP), polydispersity index (PDI), and particle size (PS) were chosen as critical quality characteristics (CQA). *The Box-Behnken design* (BBD) (*Design Expert, trial version 11.0.3.0*) recommended 17 trial runs, coded from F_1 to F_{17}, using *a design expert*, Table 1.

Based on the estimation of statistical parameters, including the multiple correlation coefficient, adjusted multiple correlation coefficient, and predicted residual sum of squares generated by the Design-Expert software, polynomial equations involving the main effect and interaction factors were determined.[22]

Preparation of Diosmin-Loaded AgNPs

AgNPs were fabricated based on a green method that involved reducing the $AgNO_3$ solution using Diosmin. Stock solutions of 5 mM of $AgNO_3$ and 0.5 mg/mL Diosmin in ethyl alcohol were used to prepare AgNPs, in which Diosmin was dispersed in ethyl alcohol. After complete dissolution, 1 mL of Diosmin solution of defined concentration was added dropwise to 10 mL of the respective $AgNO_3$ solution at the designated temperature with continuous stirring for 30 min at

Table 1 Composition and Characterization of Diosmin-Loaded AgNPs Prepared According to the Experimental Design

Formula Code	$AgNO_3$ Concentration (mM)	Diosmin Concentration (mg/mL)	Temperature (°C)	Actual PS (nm) ±SD	Predicted PS (nm)	Actual PDI ±SD	Predicted PDI	Actual ZP (mV) ±SD	Predicted ZP (mV)
F1	2.75	0.5	90	212.1±2.85	221.55	0.377±0.04	0.37	−19.6±1.51	−18.91
F2	2.75	0.3	75	243.2±8.01	256.44	0.321±0.05	0.34	−13.75±0.97	−13.32
F3	0.5	0.3	60	285.1±3.36	282.35	0.445±0.03	0.45	−10.1±0.30	−9.23
F4	5	0.1	75	265.0±8.14	261.80	0.322±0.08	0.32	−15.4±2.74	−15.44
F5	2.75	0.3	75	254.0±5.06	256.44	0.321±0.02	0.34	−13.75±1.05	−13.32
F6	5	0.3	60	187.8±7.05	172.45	0.395±0.01	0.39	−11.48±0.90	−10.99
F7	0.5	0.1	75	330.6±8.33	314.80	0.439±0.02	0.43	−10.2±0.91	−10.62
F8	0.5	0.3	90	112.2±5.81	103.45	0.315±0.06	0.32	−20.3±2.01	−20.33
F9	5	0.3	90	311.7±2.94	290.35	0.360±0.04	0.35	−12.3±1.08	−12.71
F10	2.75	0.3	75	267.0±7.03	256.44	0.352±0.03	0.34	−12.9±1.10	−13.32
F11	0.5	0.5	75	237.0±5.17	216.10	0.329±0.01	0.33	−18.2±0.85	−18.94
F12	2.75	0.1	90	208.1±2.27	228.75	0.361±0.06	0.38	−14.5±0.96	−14.13
F13	2.75	0.3	75	254.0±4.14	256.44	0.352±0.05	0.34	−12.9±2.63	−13.32
F14	2.75	0.1	60	260.9±8.47	259.25	0.473±0.01	0.4	−11.4±0.82	−11.93
F15	5	0.5	75	354.4±8.34	346.10	0.403±0.08	0.41	−7.90±1.11	−8.26
F16	2.75	0.3	75	215.8±7.72	256.44	0.340±0.01	0.34	−13.6±1.88	−13.32
F17	2.75	0.5	60	232.3±4.01	252.05	0.461±0.06	0.46	−8.12±0.93	−8.30
CK 1	2.75	0.3	90	183.5±5.23	186.05	0.321±0.08	0.335	−16.55±0.63	−16.90
CK 2	2.75	0.5	75	265.2±7.61	270.25	0.390±0.08	0.379	−13.4±0.91	−13.37
CK 3	5	0.5	60	239.3±9.22	245.55	0.419±0.07	0.467	−5.81±1.11	−5.235
CK 4	5	0.5	90	385.2±10.71	379.75	0.453±0.06	0.441	−11.88±0.95	−11.15
CK 5	2.75	0.3	60	216.5±7.43	213.64	0.399±0.03	0.423	−11.10±1.02	−10.54
F*	2.2	0.46	90	181.0±8.45	176.58	0.326±0.08	0.348	−21.45±1.27	−20.30

Notes: CK: Checkpoint formulation for experimental design model validation. F*: Optimized AgNPs formulation suggested by Design expert software.

https://doi.org/10.2147/IJN.S618588

1000 rpm. The reaction mixtures were further stirred at an ambient temperature for 2 h to allow for AgNPs ripening and stabilization. The AgNPs were stored in a refrigerator for further characterization.[23]

Characterization of the Prepared AgNPs

Determination of PS, PDI, and ZP

Dynamic light scattering (DLS) was employed to obtain the average PS, PDI, and ZP of all the colloidal dispersions of AgNPs using a Zetasizer (Nano ZS, Malvern Instruments Ltd., Malvern, UK).

All samples were sonicated for 5 min, injected into a universal foldable capillary cell possessing gold electrodes on both ends, and measured in triplicate at an ambient temperature of 25°C±0.5 with no dilution.[24] These colloidal properties were also re-estimated for the design-suggested formulation after three and six months of storage at 4°C ±0.5. Particle size values correspond to the intensity-weighted size distribution. In addition, all DLS measurements were performed in triplicate using three independently prepared nanoparticle batches to ensure reproducibility.

UV-Visible Absorbance Spectroscopy

The UV-Vis spectrum of the selected AgNPs was measured using a double-beam spectrophotometer (UV-19001, Shimadzu Industrial Systems, Kyoto, Japan) to validate the reduction of silver ions (Ag+) to AgNPs and the presence of intact Diosmin in Diosmin-loaded AgNPs.[25] The spectra were scanned, and the wavelength of maximum absorbance (λmax) was recorded at a resolution of 1 nm over a wavelength range of 200–600 nm.

The experiment was repeated three times (n = 3), and in each experiment, groups were tested in triplicate.

Energy Dispersive X-Ray (EDX) Analysis

For the analysis, the chosen formulation was introduced on a carbon-coated copper grid. A high-resolution Scanning Electron Microscope (SEM) and an energy dispersive X-ray analyzer (EDX) (Stereoscam 90 B, Cambridge Instruments-Cambridge, UK) were used at 20 kV. The samples were fully dried before being mounted on aluminum stubs with conductive carbon tape for examination. The samples were sputter-coated with a thin layer of gold to improve the surface conductivity and reduce charging effects. Spectra were collected from multiple regions, and the elemental composition was calculated using associated software.[26]

Surface Morphology Using Transmission Electron Microscopy

The PS and morphological characteristics of the selected Diosmin-AgNPs were investigated using TEM (Talos F200i, Thermo Scientific, Holland) with an accelerating voltage of 200 kV. Briefly, a few drops of the formulation were deposited on carbon-coated grids and dried under vacuum, in which no stain was required for particle visualization.[27] Photomicrographs were processed using Velox 3.3.1-19-397 software to obtain the average size of the nanoparticles.

Human Periodontal Ligament Stem Cells (hPDLSCs) Isolation

The Department of Maxillofacial Surgery at the British University in Egypt, Faculty of Dentistry, provided the impacted molars (n = 3) that were used in this study. The impacted molars were indicated for extraction from same patient (male, 20-years old), and the study was approved by the research ethics committee of The British University of Egypt (approval number: 26–021) after obtaining informed consent from the patient. After extraction, the teeth were treated with antibiotics (300 mg/mL streptomycin and 300 U/mL penicillin) in DMEM, and hPDLSCs were isolated.[28] Briefly, periodontal ligaments were broken and enzymatically digested for one hour at 37°C. Dispase II (4 mg/mL) and collagenase (3 mg/mL) were then added to the culture medium used for digestion. DMEM/F12 Ham medium was used as the culture media, with 10% FBS and 1% antibiotic/antimycotic solution added. After that, the cells were cultured at 37°C with 5% CO_2 in a humid environment. The cells were frequently observed under an inverted microscope (TCM 400; Labomed, Los Angeles, CA, USA). In this study, P4 (passage four) was used.

Characterization of the Isolated hPDLSCs

Flow Cytometric Analysis

hPDLSCs were detached by trypsinization and analyzed by flow cytometry to detect specific surface antigens.[29] The cells were extracted, treated with 4% paraformaldehyde for 15 min, cultured with a 3% bovine serum albumin solution, and then incubated with primary antibodies against CD45, CD34, CD90, CD73, CD105, and HLA-DR for one hour. After rinsing the cells with buffer, secondary antibodies (BD Biosciences, Piscataway, NJ, USA) were added and incubated at room temperature for 45 min. After three rounds of washing, the cells were evaluated using a flow cytometer (Cytofex, Beckman Coulter Inc., Brea, CA, USA).

Multilineage Differentiation

As previously reported,[30] multilineage differentiation was performed using a commercially available " human mesenchymal stem cell (MSC) functional identification kit" (R&D Systems Inc., Minneapolis, MN, USA). Supplements of specialized media for osteogenesis, adipogenesis, and chondrogenesis were included in the kit. These supplements are intended to induce stem cell differentiation into the chondrogenic, osteogenic, and adipogenic lineages. For three weeks, the cells were cultured in a 24-well plate using specific media for each type of differentiation. Alizarin Red staining was used to measure osteogenesis after the differentiation phase. Oil Red O staining solution was used to measure adipogenesis, whereas Alcian Blue staining was used to verify chondrogenic development.

Cells Viability

The cytotoxicity of $AgNO_3$, Diosmin, and AgNPs on hPDLSCs was assessed using the 3-[4, 5-dimethylthiazol-2-yl]-2, 5-diphenyl tetrazolium bromide (MTT) test. A total of 10^4 cells were seeded in 0.2 mL media per well on a 96-well plate and left to adhere overnight in an incubator. The following day, serial dilutions of $AgNO_3$, Diosmin, and AgNPs were applied to cells. For $AgNO_3$ and AgNPs, the starting concentration of the serial dilution was 64 μM (64 μM to 1 μM), while for Diosmin, the starting concentration of the serial dilution was 37.8 μM (37.8 μM to 0.3 μM). After 72 h, 100 μL/well of 5 mg/mL MTT was added, and the cells were incubated for approximately 4 h. The formazan crystals formed by viable cells were dissolved by replacing the supernatant with 100 μL/well of DMSO, and the purple color produced was measured using a microplate reader (Thermo Scientific Multiscan GO, USA) set to 570 nm. The values of each well were normalized against the control group, which consisted solely of cells and medium. The following equation was used to express the results as a percentage of cell viability:[29–31]

$$\text{Cell viability\%} = (\text{Absorbance of test}/\text{Absorbance of control}) \times 100 \quad (1)$$

The experiment was repeated three times (n = 3), and in each experiment, groups were tested in triplicate.

Osteogenic Induction and Analyses

Osteogenic Induction

Osteogenic differentiation was induced using osteogenic infuction medium which consisted of; normal culture medium supplemented with 0.1 μM dexamethasone (Sigma Aldrich, Steinheim, Germany), 10 mM β-glycerophosphate (Merck, Darmstadt, Germany), and 2.5 mg/L ascorbic acid (Sigma Aldrich, Steinheim, Germany). Cells were cultured in this osteogenic medium for 14 days. The culture medium was refreshed every 2–3 days throughout the induction period.[32] Experimental groups were defined as follows: control group where cells were cultured in standard culture medium, Osteo group where cells were cultured in osteogenic induction medium alone, $AgNO_3$ group where cells were cultured in osteogenic induction medium supplemented with 1 μM $AgNO_3$, Diosmin group where cells were cultured in osteogenic induction medium supplemented with 0.3 μM Diosmin, and the combination group where cells were cultured in osteogenic induction medium containing Diosmin-loaded AgNPs (1 μM). Treatments were maintained continuously during the entire osteogenic induction duration.

Alizarin Red S Assay

Calcified mineralized nodules were assessed in each study group at the end of the osteogenic developmental phase. After removing the culture medium, the cells were fixed at room temperature for 15 min using a 10% formaldehyde solution.

Phosphate-buffered saline (PBS) was used to wash the plates three times to remove non-adherent cells. The cells were then stained for 30 min in the dark at room temperature using a 20% Alizarin Red S solution (pH 4.2). Following staining, the cells were rinsed three times with PBS to eliminate any remaining stain and imaged using an inverted light microscope (LaboMed, USA). After dissolving the Alizarin Red staining in a 10% glacial acetic acid solution, the resulting color was quantified at 405 nm using a benchtop microplate reader.[33] The experiment was repeated three times (n = 3), and in each experiment, groups were tested in triplicate.

Alkaline Phosphatase (ALP) Activity Assay

To assess ALP activity, the cell monolayers were rinsed twice with PBS and once with 1 mL alkaline phosphatase buffer (ALPB). Each well received a milliliter of ALPB and an equivalent volume of p-nitrophenylphosphate (p-NPP), pre-cooled to 4°C. Following the addition of the p-NPP solution, aliquots (50 µL) were removed from each well and blended with an equal volume of NaOH to stop the enzyme-substrate reaction. In the current experiment, ALP converted colorless p-NPP into yellow p-nitrophenolate (p-NP), which was detected using a spectrophotometer at 405 nm. The rate of p-NP accumulation (absorbance) in each well was plotted *versus* time, and the slope of the curve in each experimental group was used to calculate the initial reaction rate, which indicates the reaction rate.[34] The experiment was repeated three times (n = 3), and in each experiment, groups were tested in triplicate.

Determination of Osteogenic-Associated Markers and Proinflammatory Markers

Real-time quantitative polymerase chain reaction (RT-qPCR) was used to investigate osteogenic-associated OPG and RUNX2, and the proinflammatory markers TNF-α and IL-1β. As per the manufacturer's instructions, total RNA extraction was carried out utilizing the RNeasy extraction kit (Qiagen) after cells (2.5×10^6 cells/group) were collected under normal conditions (37°C, 5% CO_2). The RNA samples (1 μg/sample) were retrotranscribed using the miScript Reverse Transcription Kit (QIAGEN). To demonstrate RNA purity, the ratio of sample absorbance at 260 and 280 nm was assessed using a NonoDrop spectrophotometer (ThermoFischer Scientific). Only samples with an absorbance ratio around 2 were used. cDNA synthesis conditions included, 25 °C for 5 min, 42 °C for 60 min and 70 °C for 15 min for inactivation. For cDNA amplification and quantification, real-time quantitative polymerase chain reaction (RT-qPCR) was performed using a miScript SYBR Green PCR Kit. Real-time quantitative polymerase chain reaction (RT-qPCR) was performed using the SYBR Green PCR Master Mix in final volume of 20 μL per sample. The PCR thermal cycling parameters for mRNA were 2 min at 50°C, 30s at 95°C, 35 cycles of 95°C for 10s (denaturation), 60 °C for 40s (annealing) and 72°C for 30 sec (extension). A negative control that contains all the components of the reaction except for the cDNA was included in each PCR run to detect contamination or nonspecific amplification. The results were further normalized to the reference gene GAPDH and were displayed as fold-changes by applying the $2^{-\Delta\Delta Ct}$ technique. The experiment was repeated three times (n = 3). The primer sequences used for amplification were assessed for specificity by NCBI Primer-BLAST and provided in Table 2

Table 2 Primer Sequences Used in RT-qPCR

Gene	Primer Sequence
OPG	Forward 5′-CTAATTCAGAAAGGAAATGC-3′
	Reverse 5′-GCTGAGTGTTCTGGTGGACA-3′
RUNX2	Forward 5′-GTTATGAAAAACCAAGTAGCCAGGT-3′
	Reverse 5′-GTAATCTGACTCTGTCCTTGTGGAT-3′
TNF-α	Forward 5′-ATGTTGTAGCAAACCCTCAAGC-3′
	Reverse 5′-AGGACCTGGGAGTAGATGAGG-3′
IL-1β	Forward 5′-AGCTGGAGAGTGTAGATCCCAA-3′
	Reverse 5′-TGTTTTCTGCTTGAGAGGTGCT-3′
GAPDH	Forward 5′-GGAGCGAGATCCCTCCAAAAT-3′
	Reverse 5′-GGCTGTTGTCATACTTCTCATGG-3′

https://doi.org/10.2147/IJN.S618588

Statistical Analysis

ANOVA was used to determine the significance of the model using Design Expert® 11 (StatEase, USA) following each response generated from the BBD design. Data is expressed as the mean ± standard deviation (SD) of three independently prepared nanoparticle batches (n=3). $P < 0.05$ should be present in the fitted model.[35] The lack-of-fit test was applied to assess the data fluctuation surrounding the fitted value, which should be negligible ($P > 0.05$) compared to the pure error. The multiple correlation coefficient (R^2 value) was used to express the degree of variance around the mean and was close to 1. The BBD equations were evaluated using checkpoint analysis, and equation (2) was used to calculate the percentage of bias:

$$\%\text{Bias} = \frac{(\text{Observed values} - \text{Predicted values})}{\text{Predicted values}} \text{x}100 \quad (2)$$

Regarding the in vitro biology part, normality of data distribution was tested by Shapiro–Wilk test and homogeneity of variances was estimated by Levene's test before applying parametric tests. Data is expressed as the mean ± standard deviation (SD) of three independent experiments (n=3), unless otherwise specified. Statistical analysis was performed using *Graph Pad Prism (version 5.00)* utilizing ANOVA test, followed by Tukey's post hoc analysis. Statistical significance was set at $P < 0.05$.

Results and Discussion

Isolation and Characterization of Diosmin

The ^{1}H-NMR analysis of isolated Diosmin, Figure 1 shows the resonances with coupling constants as follows: (DMSO-d6, 300 Hz); 12.93 (1H, s,5-OH), 9.46 (1H, s, 3`-OH), and in the aromatic region δ H: 7.54 (1H, dd, J = 2 Hz and 8, H 6`), 7.43 (1H, d, J=2, H-2`), 7.11 (1H, d, J=8, H-5`) corresponding to B ring. Additionally, resonances at 6.78 (1H, d, J = 2 Hz, H-8), 6.46 (1H, d, J=2, H-6), 3.86 (3H, s, 4-OCH_3), 5.08 (1H, d, J=6 Hz, H-1``), and 4.58 (1 H, H-1```) represent the anomeric proton, and 1.10 (3H, d, J=6 Hz), 2.51 (1H, H-5```), and 3.7–3.18 (m) correspond to the remaining sugar protons.

Box Behnken Design (BBD) Construction

Based on the performed preliminary study, $AgNO_3$ concentrations below 0.5 mM resulted in very low yield and weak surface plasmon resonance intensity, indicating insufficient NPs formation, whereas concentrations above 5 mM led to rapid aggregation and instability. Similarly, Diosmin concentrations higher than 0.5 mg/mL increased the viscosity of the reaction medium and promoted aggregation, while lower concentrations produced inadequate NPs stabilization. Regarding temperature, the selected range was chosen to ensure efficient NPs formation while avoiding excessive particle growth and instability at elevated temperatures.[16]

Characterization of the Prepared AgNPs

Determination of PS, PDI and ZP

The hydrodynamic diameter of the prepared AgNPs and the surface charge of the particles in the dispersion were examined by DLS. Size is a crucial factor because particles ranging between 100 and 400 nm often exhibit enhanced bioavailability compared to larger particles, demonstrating the optimal properties of osteogenic differentiation effects.[36–38] Table 1 shows that the PS for all the prepared AgNPs ranged from 112.2±5.81 to 354.4±8.34 nm and PDI values in the range of 0.32±0.02 to 0.473±0.01 showing a homogeneous particle size distribution. These values were still within acceptable ranges, as reported in literature.[39,40]

Moreover, as observed in Table 1, ZP values ranging between −7.90 to −20.30 mV were observed promoting enhanced particle stability in solution and indicating reasonable electrostatic repulsion, thus circumventing flocculation and settling of the particles as long as nonspecific integration with the negatively charged biological membranes. The bioorganic components in the plant extracts may have effectively capped AgNPs, preventing overripening, which could be the cause of the negative charges of AgNPs.[41]

Design-Expert software was used to analyze the outcomes of the experimental design. The selected independent variables, including the Diosmin concentration, $AgNO_3$ concentration, and reaction temperature, significantly affected

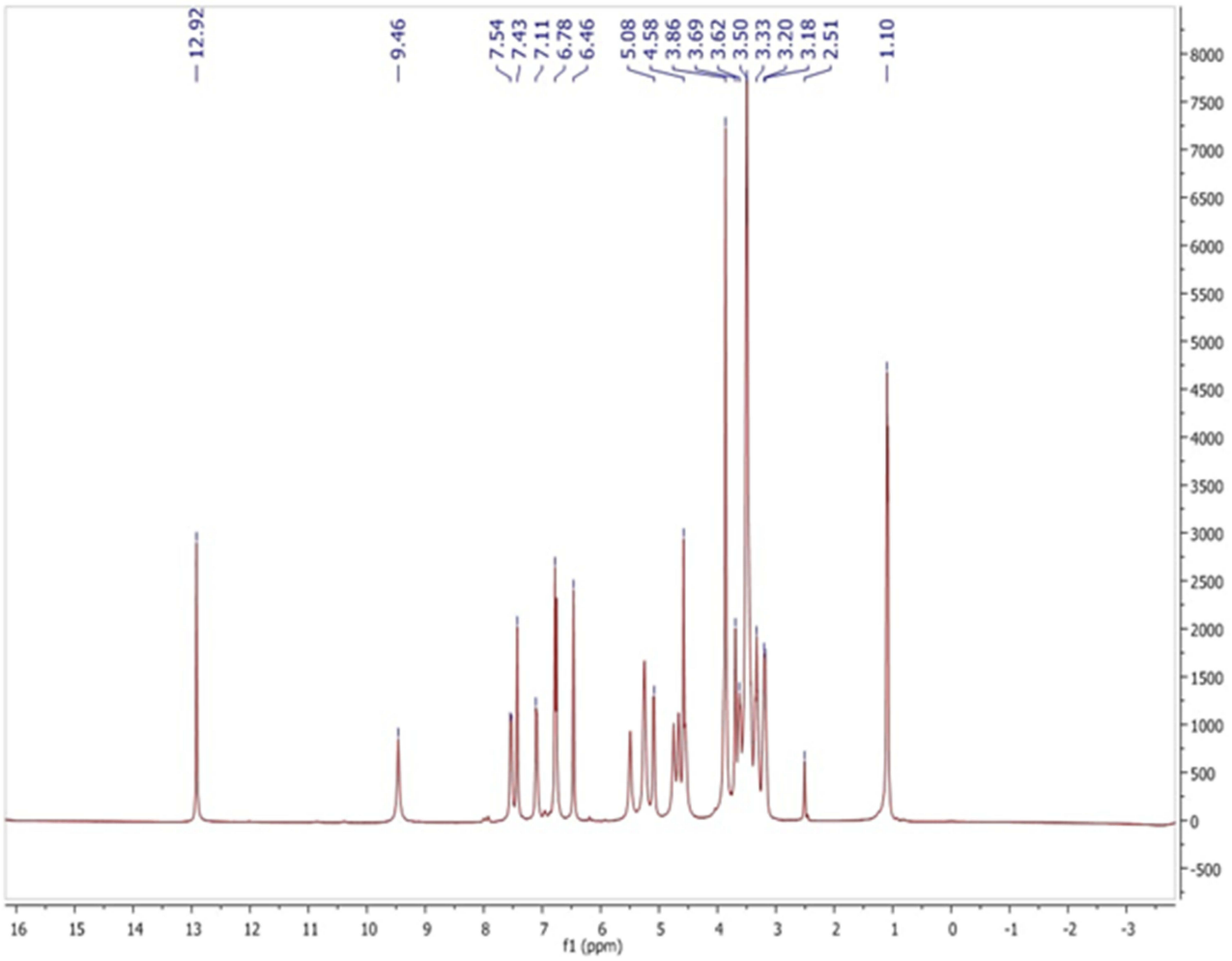

Figure 1 ^{1}H-NMR chromatogram of Diosmin.

the observed responses (PS, PDI, and ZP) of AgNPs according to a 3^3 design using BBD, as shown in Table 1. All models were significant ($P < 0.05$), as indicated by the multiple regression analysis (Supplementary Figure 2).

The "Box-Cox" plot for power transformations that demonstrates the appropriate exponent (lambda = λ) to improve the normalcy of positively or negatively skewed variables revealed no need for transformations as shown in Figure 2a–c. [42] The model was quadratic for PS, PDI, and ZP, and fell within the 95% confidence interval (CI) of the best λ value. PS had a CI ranging from −0.14 to 4.04, while PDI had a lower CI of −1.88 and a higher CI of 4.48. The CI of the ZP varied from −0.65 to 2.34. Adequate precisions of 19.067, 14.676, and 25.762 for PS, PDI, and ZP, respectively, revealed an adequate signal, indicating that the proposed model can be utilized to explore the design space. Generally, model fitting was checked via adjusted and predicted R^2 of the model as well as the Lack of Fit test to verify the model's suitability for real application.

The plot of predicted against actual values, which was utilized to provide sufficient validation of the model, is shown in Figure 2d–f. [43] Table 1 shows that there was good agreement between the anticipated and actual data for all tested colloidal properties of the AgNPs. The adjusted R^2 of the fitted model were 91.33, 92.88, and 96.76% for PS, PDI, and ZP, respectively.

Externally studentized residuals, which were calculated by dividing the raw residual by an independent estimate of its standard deviation, were computed to investigate the outliers and test the consistency of a run with the other runs.[44] "Externally studentized residuals," Figure 2g–i, exhibited no outliers among the fed data together with normally distributed results in both CQA.

https://doi.org/10.2147/IJN.S618588

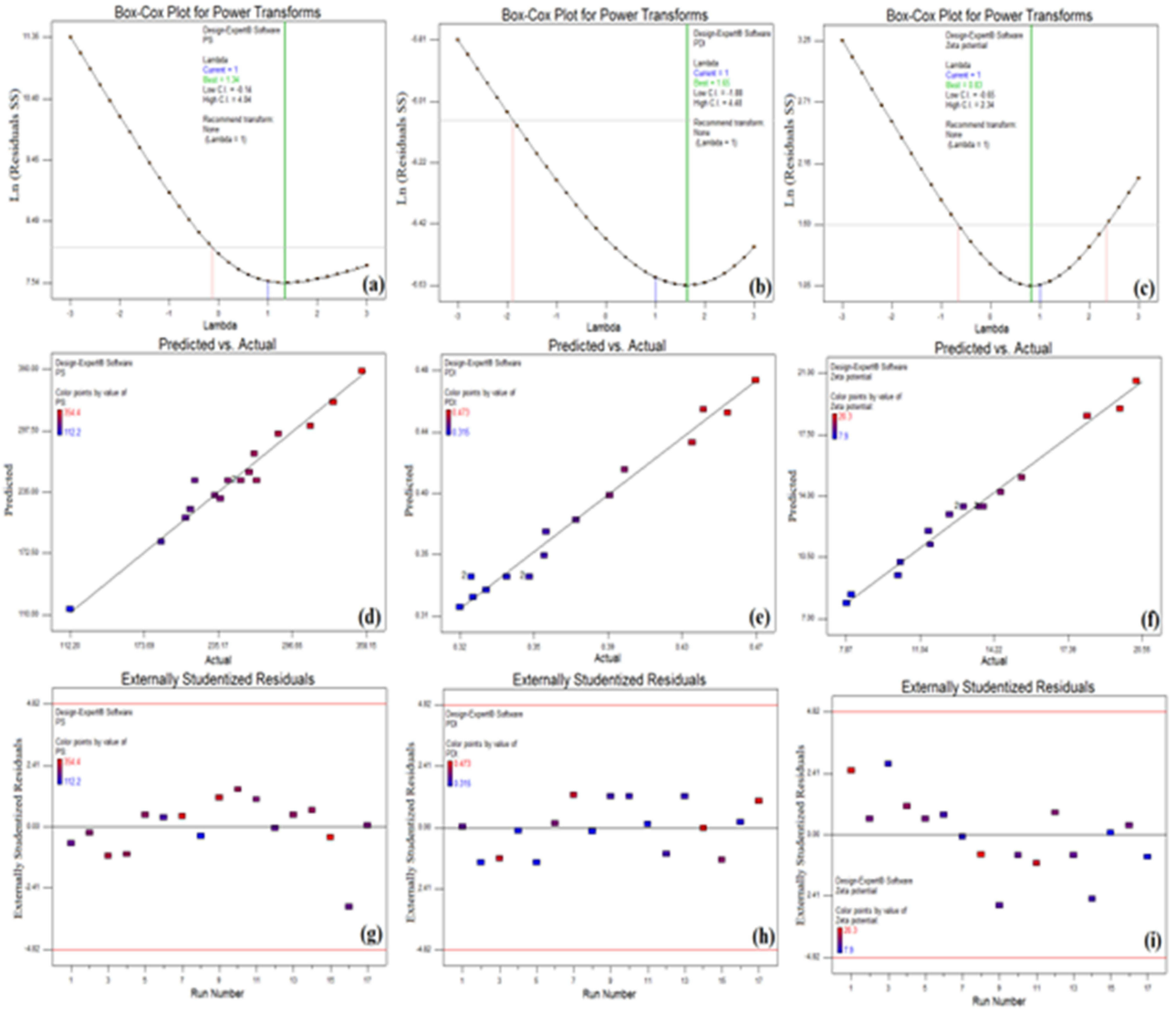

Figure 2 Box Cox plot, predicted versus actual and externally studentized residuals for PS (**a, d**, and **g**), PDI (**b, e**, and **h**) and ZP (**c, f**, and **i**) of Diosmin-loaded AgNPs.

Upon combining the individual effects of each CMA on the different CQA (Supplementary Table 1) and the interaction between different CMA evidenced by the design (Figure 3a–g), it can be concluded that the AB interaction (Figure 3a) demonstrated that a high Diosmin concentration (0.5 mg/mL) counteracted the influence of $AgNO_3$ on reducing PS. This antagonistic effect was significantly ($P < 0.05$) greater than the expected PS, as indicated by the high positive AB coefficient.[45] Moreover, increasing the $AgNO_3$ concentration may have caused a higher number of initial seeds to form, thus resulting in a small PS.[46,47]

The same observation was found in the AC interaction (Figure 3b), where higher temperature ranges resulted initially in a smaller PS, and then a significant increase in size was observed at high $AgNO_3$ concentrations ($P < 0.05$). This could be attributed to the fact that high temperatures most likely have a significant impact on nucleation and particle growth. This led to an increase in particle kinetics, resulting in more ripening and higher PS.[48,49]

Regarding PDI response, both AB and AC interactions (Figure 3c and d) were comparable to their effect on PS, where higher Diosmin concentrations and elevated temperature ranges resulted in opposing the effect of $AgNO_3$ on decreasing PDI ($P < 0.05$). The lack of a capping agent that would have shielded the AgNPs nuclei from excessive Ostwald ripening was the cause of the rise in PS triggered by the increase in Diosmin concentration.[45] Increasing the

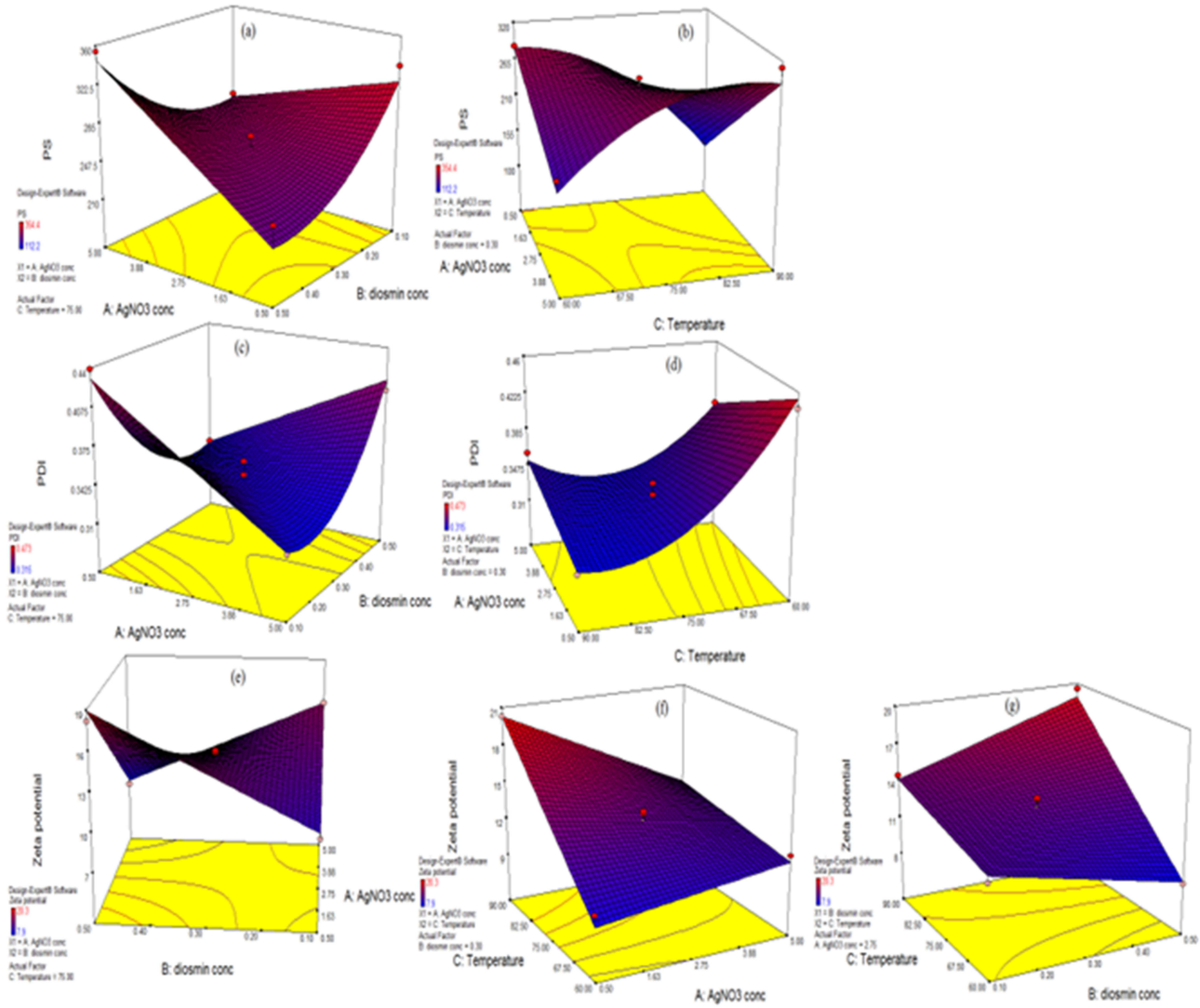

Figure 3 Interactions for PS (**a**: AB interaction, **b**: AC interaction), PDI (**c**: AB interaction, **d**: AC interaction), and ZP (**e**: AB interaction, **f**: AC interaction, and **g**: BC interaction) of Diosmin-loaded AgNPs.

temperature is always associated with higher PS ranges because of its influence on nucleation kinetics and acceleration in nanoparticle growth, leading to a larger particle size during synthesis.[48]

For ZP, three interactions were significant. The AB interaction resulted in opposing the effect of $AgNO_3$ in imparting more surface charges ($P < 0.05$) (Figure 3e). High temperature ranges resulted in a sharper drop in ZP with increasing $AgNO_3$ concentration ($P < 0.05$) (AC interaction, Figure 3f). [50] The opposite was observed in BC interaction, where higher temperature ranges opposed the effect of increasing Diosmin concentration on decreasing ZP,[51] resulting in a significant increase in the surface charges of the NPs ($P < 0.05$) (Figure 3g). [52] The temperature probably affected the viscosity, ion mobility, and electrical double-layer behavior, in addition to its impact on the nucleation and growth of $AgNO_3$, resulting in an increase in the ZP value.[53]

Checkpoint analysis was performed to assess the equations generated by the design. The analysis was conducted using five random Diosmin-AgNPs formulations with respective compositions, as shown in Table 1. Their PS, PDI, and ZP were experimentally determined and computed using equations (3), (4), and (5), Table 3. The respective % bias, computed by equation (2) ranged between 1.338 to 2.545% for PS, 2.04 to 10.06% for PDI, and 0.22 to 11.08% for ZP, displaying insignificant differences ($P > 0.05$) and establishing the reliability of the implicated design.

https://doi.org/10.2147/IJN.S618588

Table 3 Model Summary Statistics for PS, PDI, and ZP of Diosmin-Loaded AgNPs

Term	Description/Value in PS	Description/Value in PDI	Description/Value in ZP
Model order	Quadratic	Quadratic	Quadratic
P-value	0.0004	0.0002	0.0002
Lambda (λ)	1	1	1
Transformation	None	None	None
R2	0.9569	0.9632	0.8953
Adjusted R^2	0.9137	0.9346	0.8324
Predicted R^2	0.8091	0.8776	0.7030
Adequate precision	20.143	16.134	12.884
Equation	$PS = -200.18719 - 211.71235* A - 703.33333 * B + 23.27074* C + 101.66667 * AB + 2.19852* AC + 4.52346 * A^2 + 676.25000* B^2 - 0.20222 * C^2$ (Eq. 3)	$PDI = +1.95718 - 0.087278 * A - 0.86746 * B - 0.033392 * C + 0.10611 * AB + 7.03704E - 004* AC + 0.93026 * B^2 + 1.89825E - 004 * C^2$ (Eq. 4)	$ZP = -7.0214 + 7.14333 * A + 27.38194 * B + 0.19457 * C - 8.61111 * AB - 0.069481 * AC - 0.70000 * BC$ (Eq. 5)

Abbreviations: PS, Particle size; PDI, Poly dispersity index; ZP, Zeta potential.

https://doi.org/10.2147/IJN.S618588

A desirability study was conducted based on the results of PS, ZP, and PDI to select the optimized AgNPs formulations. The BBD suggested the following formulation with composition: 2.2mM of $AgNO_3$, Diosmin concentration (0.46 mg/mL) and temperature of 90°C, showing the highest desirability value of 0.751 and was coded F*. The practically assessed PS, PDI, and ZP values displayed insignificant differences relative to the expected values ($P > 0.05$).[39,40] Accordingly, F* (with PS of 181±8.45 nm, PDI 0.326±0.082, and ZP −21.45±1.27 mV) was subjected to subsequent comprehensive characterization studies (Figure 4a and b).

Meanwhile, the colloidal properties (PS, PDI, and ZP) of F* showed non-significant changes ($P > 0.05$) after three months' storage at 4°C (190.76±12.9 nm, 0.361±0.09, and −20.97±2.31 mV for PS, PDI, and ZP, respectively), indicating good stability of the colloidal dispersions. However, significant increases in PS and PDI (278±20.5 nm and 0.588±0.10, respectively) and a decrease in ZP (−12.8±2.03 mV) ($P < 0.05$) were noted only after 6 months of storage. This could be attributed to the fact that lowering the ZP can lead to more particle aggregation, yielding a larger particle size. The significant increase in PDI confirmed the presence of a mixture of the original sized particles together with ripened particles upon storage, resulting in a heterogeneous distribution.[54]

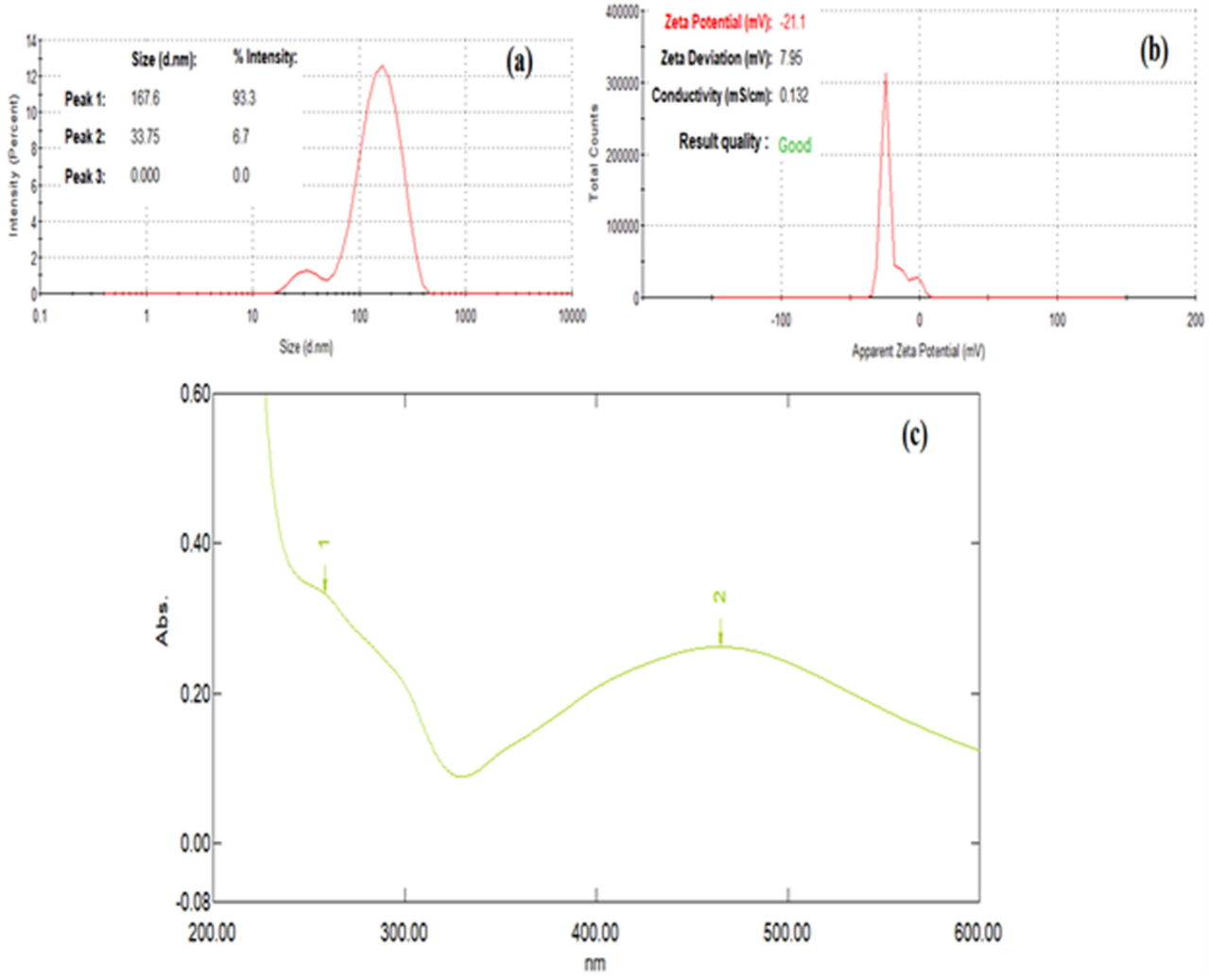

Figure 4 Representation of (**a**) Particle size, (**b**) Zeta potential, and (**c**) UV-visible spectra of the optimized AgNPs (F*). Peak 1: Maximum absorbance of Diosmin is presented at λ =270 nm. Peak 2: Maximum absorbance of AgNPs is presented at λ = 465 nm.

https://doi.org/10.2147/IJN.S618588

UV-Visible Absorbance Spectroscopy

UV-visible spectroscopy is one of the most reliable, simple, sensitive, and useful techniques for the characterization and subsequent confirmation of the formation of Diosmin-loaded AgNPs. The colloidal dispersion of the prepared AgNPs exhibited a dark orangish-brown color owing to the unique interaction with certain wavelengths of light.[55] The conduction and valence bands of AgNPs were located relatively close to each other, allowing electrons to flow freely. By virtue of the collective oscillation of AgNPs electrons in resonance with the light wave, these free electrons generate what is called a surface plasmon resonance (SPR) absorption band.[56,57] The UV-visible spectra of F* displayed a characteristic SPR absorption band between 400 and 500 nm[58–60] as shown in Figure 4c. The maximum absorbance was observed at λ = 465 nm, indicating the successful reduction of Ag + ions to metallic silver. The observed good colloidal stability along with the sharp intense peaks indicates a uniform particle distribution, confirming the absence of significant aggregation, as aggregated particles would show broader, red-shifted peaks. The Diosmin peak appeared at 270 nm, ensuring that the Diosmin molecule preserved its structural integrity under the experimental conditions used in the green synthesis of Diosmin-based AgNPs.[61]

Meanwhile, the observed size–wavelength relationship for AgNPs was found to be consistent with established correlations for *the Mie* scattering theory and within the reported ranges. According to previous studies, particles of 200 nm usually showed SPR maxima in the 440–460 nm range.[62]

Energy Dispersive X-Ray (EDX) Analysis

EDX analysis was carried out to define the elemental composition of the biosynthesized AgNPs using Diosmin as a reducing and capping agent. The presence of only the expected elements (Ag, C, and O) confirmed the successful green synthesis of undesired byproducts. A strong distinctive EDX spectrum was observed at 3 keV (Figure 5a), which is typical for the absorption of AgNPs due to SPR, confirming the successful biosynthesis of AgNPs using Diosmin, where the existence of the elemental metal signal was verified.[63] Other peaks for oxygen and carbon were noted. The C signals (16.19 weight%) may be due to the carbon-coated copper grid used to prepare the sample or may be attributed to the carbon atoms present within the Diosmin molecule itself.[64] Oxygen signals (66.58%) may have originated from phytochemical compounds in the aqueous extract that were close or attached to the surface of the nanoparticles. Since Diosmin has several hydroxyl (-OH) and methoxy ($-OCH_3$) groups in its flavonoid structure, the high oxygen percentage showed that it effectively could serve as a capping and reducing agent, guaranteeing the potential bioactivity of surface-bound flavonoid molecules.[65] As mentioned in a previous study, this could be due to the -OH groups in flavonoids, which can be released during the tautomeric transition of flavonoids from enol to keto type, releasing reactive hydrogen atoms causing AgNPs reduction. This mechanism is directly related to Diosmin, which contains comparable hydroxyl groups.[66] The presence of 17.23% of silver content provided strong evidence of successful AgNPs formation. This came in consistent with data reported in the literature for plant-mediated synthesis of $AgNO_3$, where the presence of organic capping agents typically resulted in a yield of 10–20% Ag^+.[25,67,68] Signals corresponding to Ag, C, and O were attributed to the nanoparticle formulation, whereas any contributions originating from the support grid or coating materials were excluded from the compositional interpretation.

Surface Morphology Using Transmission Electron Microscopy

The morphological characteristics of the selected F*formulation were examined using TEM analysis. TEM photomicrographs revealed that Diosmin-AgNPs were spherical and uniformly distributed without aggregation, with a PS of 150–160 nm (Figure 5b and c). Similar results were obtained by *Iravani* et al,[69] who prepared AgNPs with sizes ranging from 150 to 260 nm using m-hydroxybenzaldehyde as a reducing agent. The PS obtained using the TEM technique was commonly smaller than that obtained using the DLS technique (181.0±8.45 nm) as TEM measures the actual PS of the sample in its dried state, whereas DLS measures the average hydrodynamic PS in aqueous media.[70] This was in accordance with *Khedr* et al,[71] who reported a remarkable difference between the mean PS assessed using the two techniques for AgNPs produced using *Cynara scolymus L* crude extracts. This size range indicates good stability against aggregation while maintaining a sufficient surface area for biological activity.

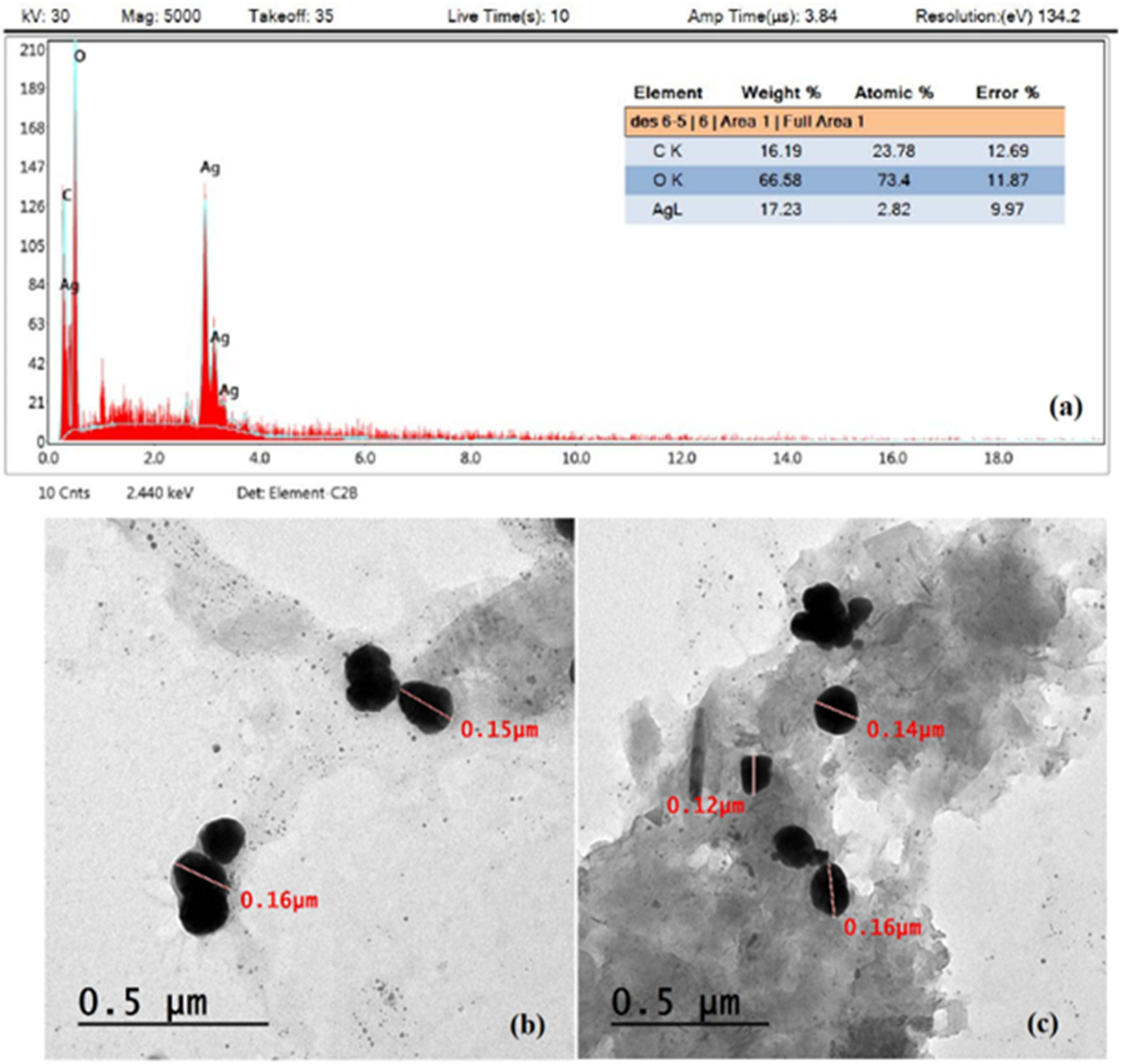

Figure 5 Energy dispersive X-ray and Transmission electron microscopy assessment of the optimized AgNPs (F*). (**a**): Energy dispersive X-ray. (**b**) and (**c**): Transmission electron microscopy images of the selected AgNPs (F*).

Characterization of the Isolated hPDLSCs

Flow Cytometric Analysis

MSC markers (CD105, CD73, and CD90) were positively expressed (> 95%) in the isolated cell population according to flow cytometric analysis, whereas hematopoietic stem cell markers (HLA-DR, CD43, and CD34) were negatively expressed (< 3%) (Figure 6a). The separated cells exhibited MSC traits including adhesion to plastic surfaces and spindle shape.

Multilineage Differentiation

The isolated cells were able to develop into osteoblasts, as confirmed by the mineralized nodules positively stained with Alizarin Red stain, chondrocytes confirmed by the proteoglycan matrix positively stained with Alizarin blue stain, and the adipocytes confirmed by the oil droplets positively stained by Oil Red stain (Figure 6b).

https://doi.org/10.2147/IJN.S618588

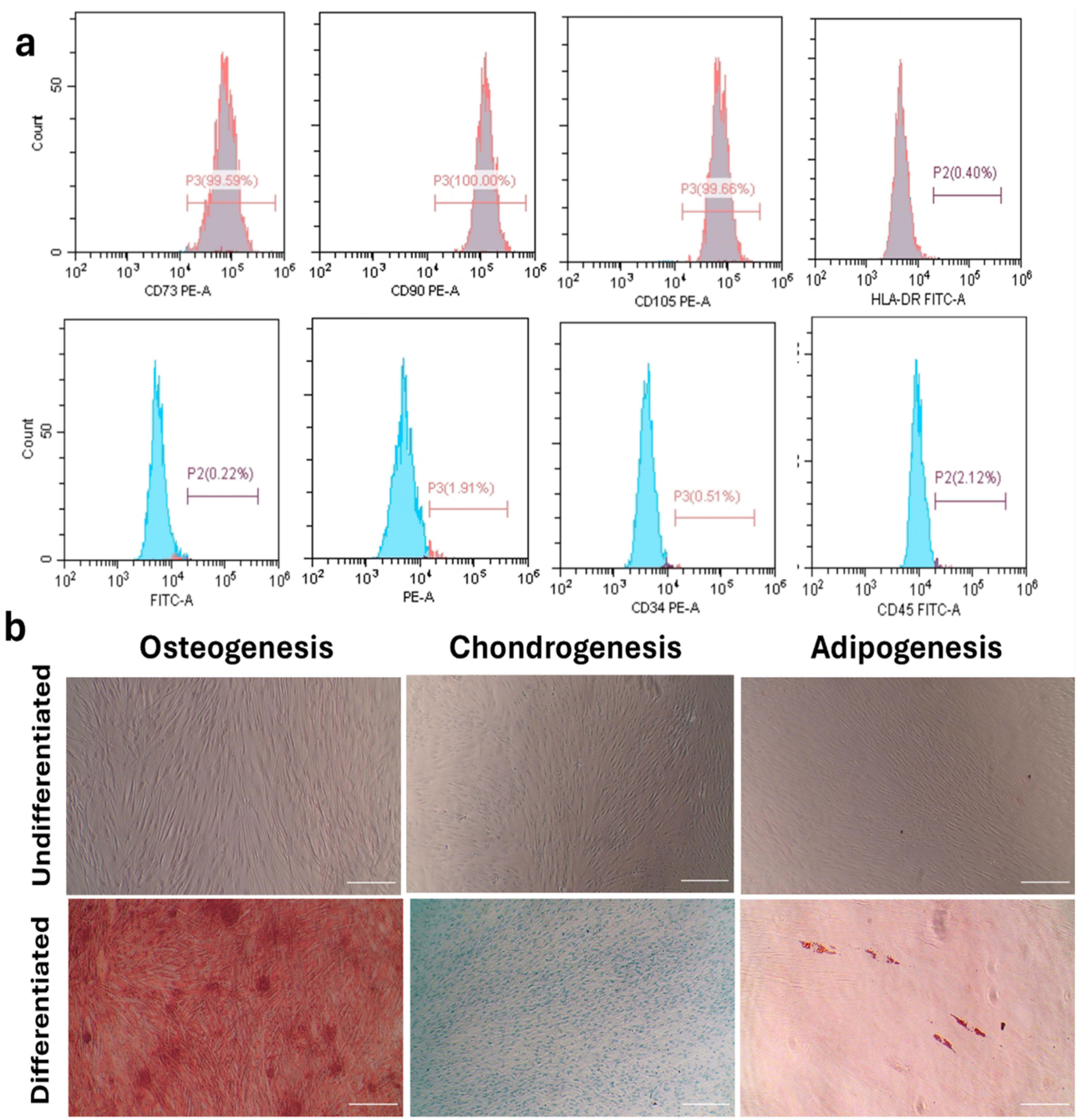

Figure 6 Stem cell characterization results. (**a**) Flow cytometry results showing positive expression of stem cell CDs and negative expression of hematopoietic CDs. (**b**) Multilineage differentiation of stem cells into osteocytes, chondrocytes, and adipocytes. Original magnification: 100 ×; Scale bar: 250 μm.

Cell Viability

Orthopedists face significant challenges in managing extensive bone defects, especially those caused by infection, severe trauma, tumor or cyst removal, or therapeutic failure.[72] Various methods have been developed to overcome these issues and repair lost bones.[73] Modern methods mainly concentrate on increasing bone regeneration capacity to overcome the inherent drawbacks of using autografts, allografts, and xenografts. This can be achieved by employing cells that can generate bones when applied alone or in conjunction with an osteoconductive scaffold to skeletal deficiency[74] or by applying biologically active materials.[75]

Researchers are urged to experimentally confirm the effectiveness of Diosmin against other illnesses such as osteoporosis, as it is safe for human use. Thus, the anti-osteoporotic effects of Diosmin have been previously studied. Sharma et al[76] and Hu et al[77] demonstrated that Diosmin prevented bone loss in rats with chronic kidney disease and ovariectomy, respectively. Additionally, in a rat femur osteotomy model, a mixture of hesperidin and Diosmin improved bone regeneration.[78] Research on bone tissue engineering has relied heavily on nanomaterials.[9] External fixation is still required, even though the bone can self-regenerate and remodel in many situations such as infection, severe trauma, tumor, or cyst excision.[79,80] AgNPs were used to examine their osteogenic effects on hPDLSCs. Prior to assessing toxicity or cytocompatibility, the size, shape, and stability of the nanoparticles were evaluated, as previously discussed.

According to Zhang et al[81] and Kumar et al,[82] AgNPs exhibited proliferative and osteogenic differentiation-inducing effects on MSCs and promoted fracture healing. They claimed that AgNPs could induce the proliferation of MSCs and fibroblasts, MSCs osteogenic differentiation, and chemo-attract MSCs and fibroblasts to migrate to the fracture site to aid in the development of the fibrous joint and eventually, healing of the fractured bone.

In the present study, cell viability was assessed using the MTT assay after cells were treated with serial dilutions of $AgNO_3$, Diosmin and AgNPs (64–1 μM, 37.8–0.295 μM and 64–1 μM, respectively) for 72 h to investigate their impact on hPDLSCs viability. It was observed that $AgNO_3$ and AgNPs decreased the viability of hPDLSCs in a dose-dependent manner (Figure 7a–c).

The osteogenic effects of $AgNO_3$ and AgNPs were compared at a dose of 1 μM, which showed no cytotoxicity on hPDLSCs when serial dilutions of both treatments were used in the MTT assay. As previously stated, Diosmin was used in the formulation with a concentration of 0.3 μM according to BDD. To the best of our knowledge, this is the first attempt to demonstrate the osteogenic effects of Diosmin-capped AgNPs using Diosmin as a reducing agent on hPDLSCs viability and osteogenic differentiation potential in vitro.

Osteogenic Analyses

Alizarin Red S Assay

The current study evaluated the osteogenic potential of $AgNO_3$, Diosmin, and AgNPs in hPDLSCs using various assays, including Alizarin Red S and ALP assays. Additionally, the expression of osteogenic markers (OPG and RUNX2) and pro-inflammatory markers (TNF-α and IL-1β) were assessed using RT-qPCR.

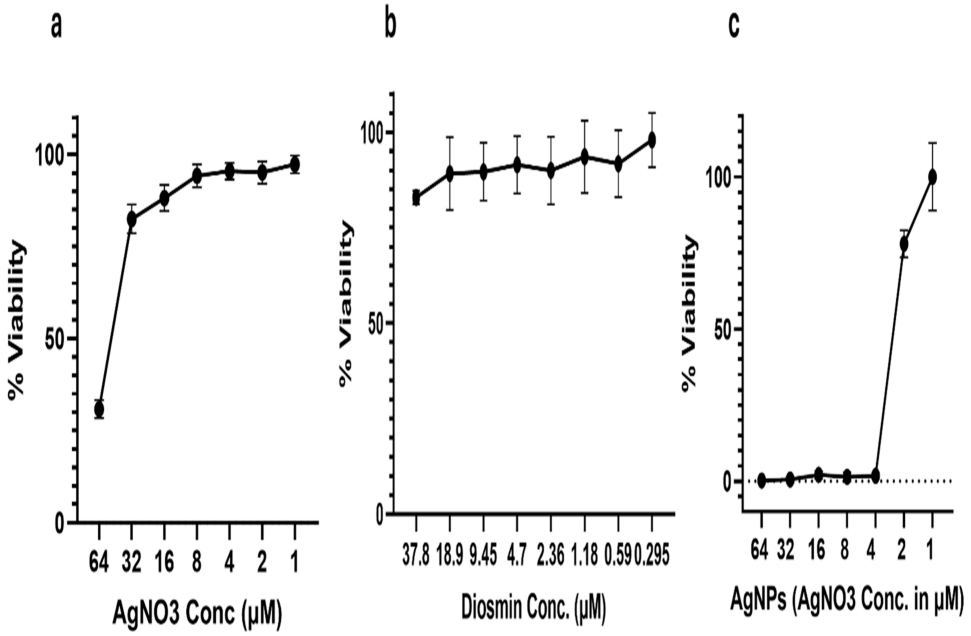

Figure 7 MTT assay showing the effect of different concentrations of (**a**) $AgNO_3$, (**b**) Diosmin, and (**c**) AgNPs on hPDLSCs viability.

https://doi.org/10.2147/IJN.S618588

The Alizarin Red S assay, an in vitro test, was utilized to measure the calcified nodules produced to evaluate the osteogenic activity of the differentiated cells (Figure 8a). Mineralization was significantly better in the AgNPs and Diosmin groups compared to the $AgNO_3$, osteogenic, and control groups ($P < 0.0001$). No significant difference in mineralization was observed in the $AgNO_3$ group compared to the osteogenic group. AgNPs group showed higher mineralization compared to Diosmin group, however, it was non-significant statistically ($P > 0.05$) (Figure 8b).

Alkaline Phosphatase Activity Assay

The ALP assay, used to calorimetrically measure ALP activity, which is a crucial enzyme for osteoblast development and mineralization, further confirmed the results of the Alizarin Red S assay. Similarly, ALP activity followed the same pattern as that of the Alizarin assay. A significant increase in ALP activity in the AgNPs group was noted compared to the Diosmin ($P = 0.0023$), $AgNO_3$ ($P < 0.0001$), osteogenic ($P = 0.0005$), and control ($P < 0.0001$) groups. On the other hand, no significant differences were observed in ALP activity in the Diosmin group, $AgNO_3$ and osteogenic groups ($P > 0.05$) (Figure 8c and d).

In accordance with our findings, Chandran et al[83] reported the bone formation effect of gelatin and nanohydroxyapatite scaffolds both in vitro and in vivo. They found that Diosmin improved the scaffold's capacity for osteoblast development and differentiation in mouse MSCs at both the cellular and molecular levels by activating FAK, ERK, and

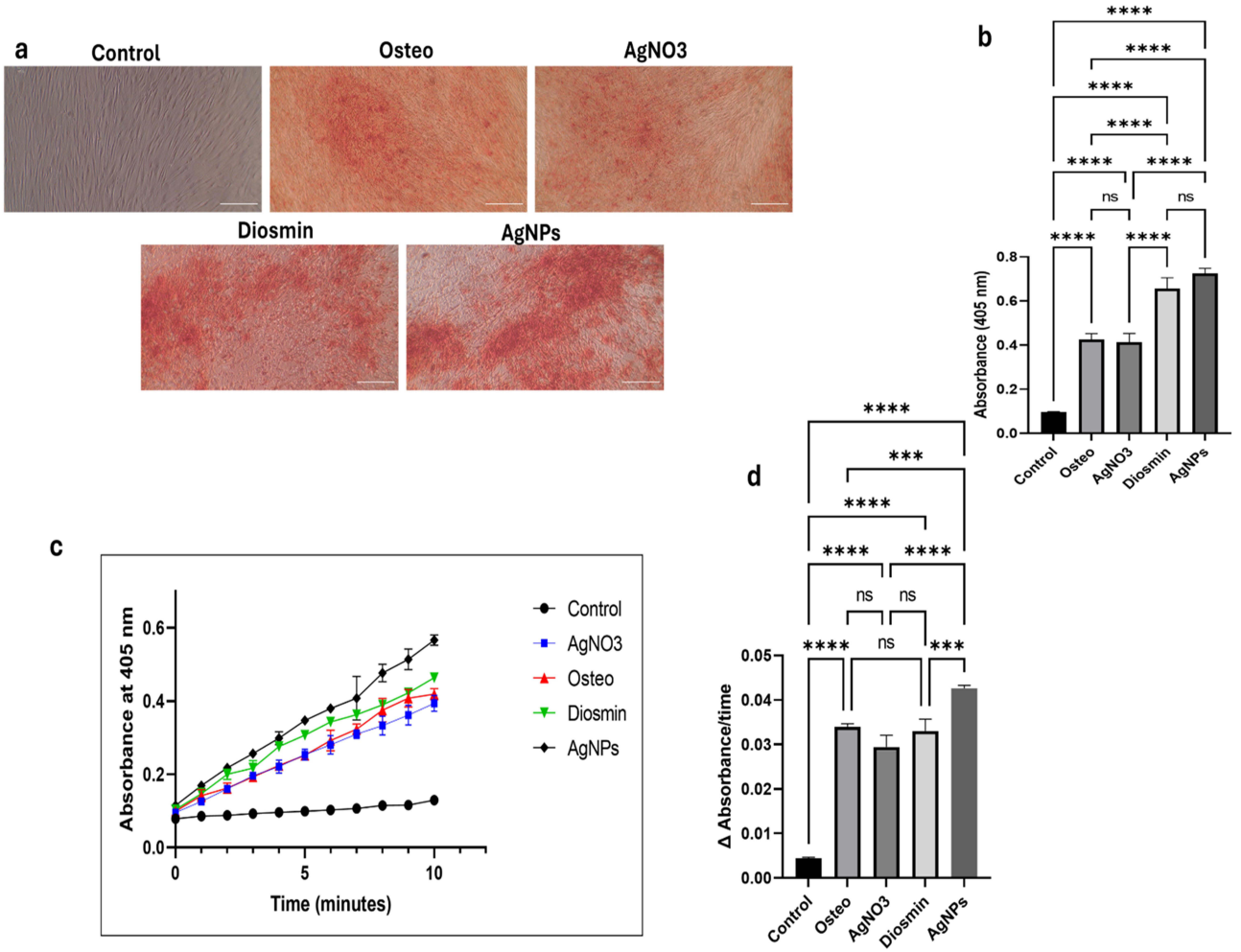

Figure 8 Assessment of osteogenic differentiation using mineralization (Alizarin Red staining) and enzymatic (ALP) activity assays after 21 days of osteogenic induction in the studied groups. (**a**) Representative images of mineralized nodules. (**b**) Statistical analysis of the degree of mineralization in the groups. (**c**) Typical ALP assay kinetic profile showing the accumulation of the yellow p-nitrophenolate product over time in the different groups. (**d**) The rate of yellow p-NP accumulation was compared among the study groups by calculating the slope of each reaction. The provided values represent the mean ± SD of three separate experiments. *** indicates significance of $P < 0.001$, **** indicates significance of $P < 0.0001$ and NS indicates non-significance ($P > 0.05$).

https://doi.org/10.2147/IJN.S618588

RUNX2 expression. In an osteogenesis animal model, Zhang et al[81] found that AgNPs promoted fracture repair and demonstrated proliferative and osteogenic differentiation-inducing effects on MSCs. They suggested that AgNPs may facilitate the development of callus and the subsequent end-joining of the fractured bone in several ways, including chemo-attracting fibroblasts and MSCs to migrate to the fracture site, inducing MSCs proliferation, and MSCs osteogenic differentiation by stimulating TGF-β/BMP signaling in MSCs.

Determination of Osteogenic-Associated Markers and Proinflammatory Markers

The current study utilized RT-qPCR to compute the expression of osteogenic markers, such as OPG, a soluble decoy receptor that prevents the activation and development of osteoclasts,[84] and RUNX2, a transcription factor necessary for osteoblast proliferation and differentiation.[85] OPG expression was significantly increased in AgNPs and Diosmin groups compared to $AgNO_3$ and osteogenic groups ($P < 0.05$). (Figure 9a). Similarly, RUNX2 expression levels were significantly higher in AgNPs and Diosmin groups compared to $AgNO_3$ group ($P < 0.05$) (Figure 9b). Our results indicate the enhanced osteogenic effect of the Diosmin-capped AgNPs compared to the conventional $AgNO_3$ formulation.

In agreement with our findings, Arafa et al[86] stated that Diosmin inhibited the formation of ROS and RANKL, prevented bone resorption, and enhanced bone production by upregulating BCL2, RUNX2, Wnt, p-Akt, osteocalcin, and

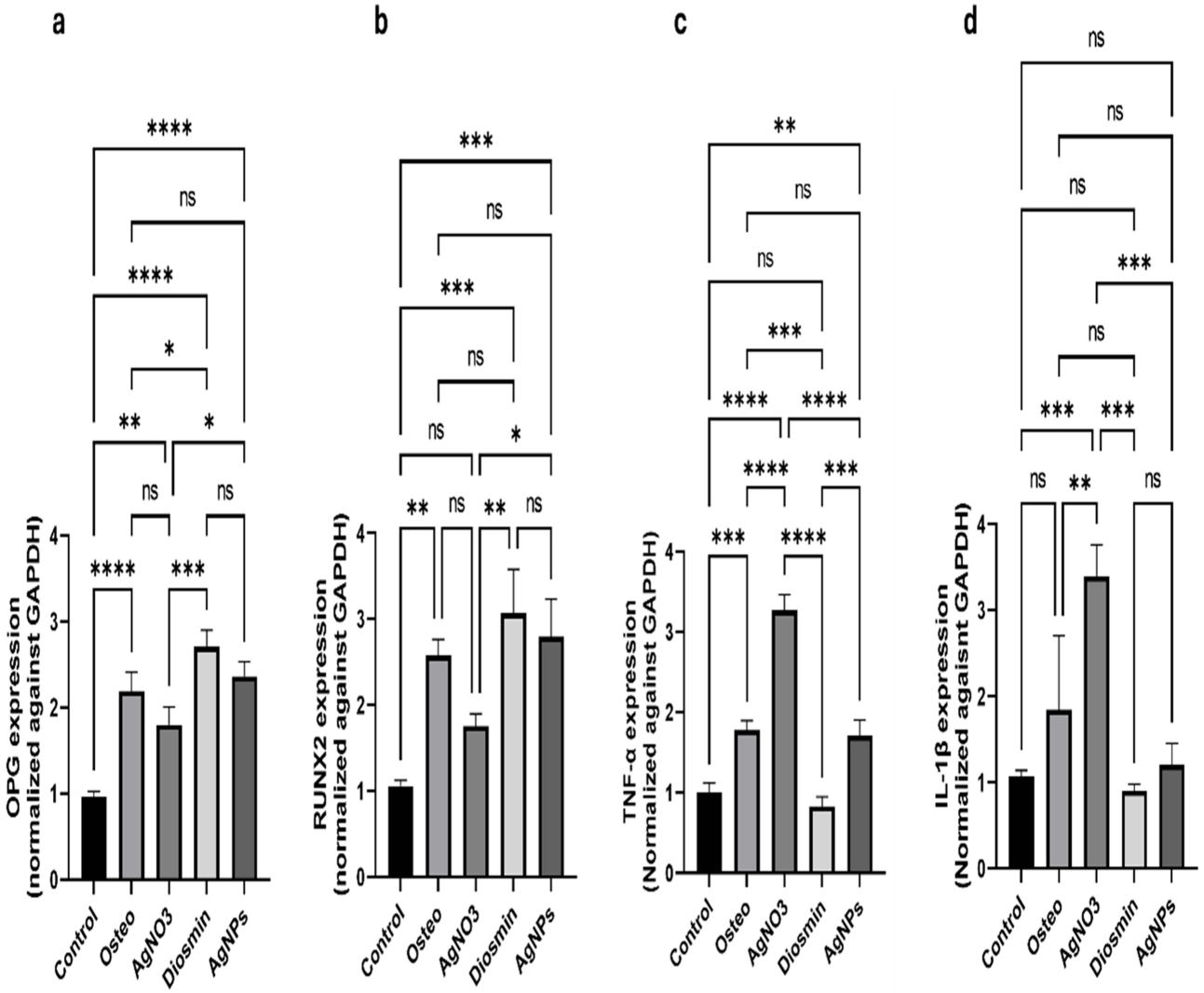

Figure 9 Relative expression levels of osteogenic and proinflammatory markers in the studied groups. (**a**) OPG, (**b**) RUNX2, (**c**) TNF-α and (**d**) IL-1β, represented as mean ± SD. * indicates significance of $P < 0.05$, ** indicates significance of $P < 0.01$, *** indicates significance of $P < 0.001$, **** indicates significance of $P < 0.0001$. NS indicates non-significance ($P > 0.05$).

https://doi.org/10.2147/IJN.S618588

OPG. Another study found that AgNPs caused cell shrinkage and increased RUNX2 and RANKL expression. However, in contrast to the current study, AgNPs decreased OPG expression.[87]

To evaluate the anti-inflammatory effects, the expression levels of TNF-α and IL-1β (pro-inflammatory markers) were examined using RT-qPCR in all study groups. TNF-α showed lowest expression in Diosmin group compared to osteogenic ($P < 0.001$) and $AgNO_3$ ($P < 0.0001$) groups. TNF-α expression in AgNPs group was significantly decreased compared to $AgNO_3$ group ($P < 0.001$), denoting the decreased expression of inflammatory markers after using Diosmin as a reducing agent (Figure 9c). Similarly, the expression of IL-1β was significantly higher in $AgNO_3$ group than in the osteogenic and control groups ($P < 0.01$, $P < 0.001$, respectively) while IL-1β expression was substantially reduced in Diosmin and AgNPs groups compared to that in $AgNO_3$ group ($P < 0.01$) (Figure 9d).

In line with our findings, Sabry et al[37] demonstrated the anti-inflammatory properties of AgNPs as well as their influence on enhancing the osteogenesis process in rat mandibular critical size defects, indicating that bone repair may be aided by controlling local inflammatory responses. In addition, Shalkami et al[88] assessed the anti-inflammatory properties of Diosmin and reported that Diosmin therapy reduced the development of ulcerative colitis based on its capacity to reduce inflammation, oxidative stress, and apoptosis in the rat colon by lowering the expression of caspase-3, oxidative stress markers, and inflammatory markers (TNF-α, COX-II, and MPO).

The in vitro study demonstrated that $AgNO_3$ and AgNPs were able to reduce hPDLSCs viability in a dose-dependent manner, with no cytotoxicity observed at 1 μM, suggesting that the biological effects of AgNPs are highly concentration dependent. Diosmin alone and Diosmin-capped AgNPs significantly enhanced osteogenic differentiation, as evidenced by increased mineralization and ALP activity compared to $AgNO_3$, osteogenic, and control groups. Diosmin-capped AgNPs notably elevated ALP activity compared with the other groups. Also, RT-qPCR results showed upregulation of osteogenic markers OPG and RUNX2, particularly in AgNPs and Diosmin groups. Finally, the use of Diosmin as a reducing agent had a positive effect by decreasing the expression of inflammatory markers. These results support its potential role in promoting osteoblastic differentiation and modulating inflammatory response.

Conclusion

In the current study, Diosmin was successfully isolated and prepared into AgNPs using green methods which were further optimized based on the Box-Behnken design of experiments and showed favorable physicochemical properties such as nanosized particle distribution, negative surface charge and acceptable stability. The optimized Diosmin-loaded AgNPs enhanced hPDLSC osteogenic differentiation and decreased inflammatory markers compared to $AgNO_3$ and free Diosmin, suggesting their possible role in promoting osteogenesis and healing via the control of inflammatory response. The results of our study provide a solid basis for further studies on green produced Diosmin-loaded AgNPs as potential biomaterials for bone regeneration therapies.

Study Limitations

The current study has certain limitations that must be acknowledged. While AgNPs exhibited encouraging biological activity, the possible toxicity linked to AgNPs and the role of liberated Ag^+ ions were not explicitly examined and necessitated additional evaluation. The present investigation did not encompass a thorough evaluation of Diosmin loading efficiency and release kinetics, which should be examined in subsequent research. Measuring markers on protein level could validate the results. Furthermore, the study is limited to in vitro evaluation, though in vivo validation in a critical-size bone defect model and direct comparison with established osteogenic inducers, such as BMP-2, would greatly enhance translational evidence. Moreover, in the present study, using Diosmin as a reducing agent in the preparation of AgNPs modulated the inflammatory response to $AgNO_3$, however further mechanistic and dose-optimization studies are needed to confirm the results and to better define their therapeutic safety window. Consequently, in vivo investigations are essential to confirm the safety, therapeutic efficacy, and clinical significance of the proposed system.

Abbreviations

hPDLSs, Human periodontal ligament stem cells; ALP, Alkaline phosphatase; Ag+, Silver ions; AgNO3, Silver nitrate; AgNPs, Silver nanoparticles; ALPB, Alkaline phosphatase buffer; ANOVA, Analysis of variance; BBD, Box-Behnken design; BMPs, Bone morphogenetic proteins; CMA, Critical material attributes; CQA, Critical quality attributes; CRP, C-reactive protein; DLS, Dynamic light scattering; DMEM, Dulbecco's Modified Eagle Medium; DMSO, Dimethyl sulphoxide; EDX, Energy dispersive X-ray analyzer; FBS, Fetal bovine serum; MSC, Mesenchymal stem cell; MTT, 3-[4,5-dimethylthiazol-2-yl]-2,5-diphenyl tetrazolium bromide; NaOH, Sodium hydroxide; OPG, Osteoprotegerin; p-Akt, Phosphorylated Akt; PBS, Phosphate-buffered saline; PDI, Polydispersity index; p-NP, p-nitrophenolate; p-NPP, para-nitrophenylphosphate; PS, Particle size; RANKL, Receptor activator of nuclear factor κB ligand; ROS, Reactive oxygen species; RT-qPCR, Real-time quantitative polymerase chain reaction; RUNX2, Runt-related transcription factor 2; SEM, Scanning Electron Microscope; SPR, Surface plasmon resonance; TEM, Transmission Electron Microscopy; ZP, Zeta potential.

Data Sharing Statement

The data supporting the findings of this study are available from Shymaa Hatem, the corresponding author upon reasonable request.

Acknowledgments

The authors confirm that no acknowledgments are relevant to this work.

Author Contributions

All authors made a significant contribution to the work reported, whether that is in the conception, study design, execution, acquisition of data, analysis and interpretation, or in all these areas; took part in drafting, revising or critically reviewing the article; gave final approval of the version to be published; have agreed on the journal to which the article has been submitted; and agree to be accountable for all aspects of the work.

Disclosure

The authors report no conflicts of interest in this work.

References

1. Dos Santos RL, Ahmed A, Hunn BE. et al. Oxidation-responsive, settable bone substitute composites for regenerating critically-sized bone defects. *Biomater Sci*. 2025;13(8):1975–1992. doi:10.1039/D4BM01345J
2. Ivanova N, Ivanov S, Peev S, Dikova T. Types of Bone Substitutes and Their Application in Regenerative Medicine: a Systematic Review. *J Funct Biomater*. 2025;16(9):341. doi:10.3390/jfb16090341
3. Zhang J, Zhang W, Yue W, Qin W, Zhao Y, Xu G. Research Progress of Bone Grafting: a Comprehensive Review. *Int J Nanomed*. 2025;20:4729–4757. doi:10.2147/IJN.S510524
4. Romain P, Barahona I, Catarina I, Romero A, Mascarenhas P. Regenerative Applications and Performance of Periodontal Ligament Stem Cells: a Comprehensive Review of In Vivo Studies. *Appl Sci*. 2025;15(21):11444. doi:10.3390/app152111444
5. Liang X, Zhang Z, Fang S, et al. Three-dimensional scaffold-free periodontal ligament stem cell pellets for alveolar ridge preservation: an in vitro and in vivo study. *BMC Oral Health*. 2025;25(1):1227. doi:10.1186/s12903-025-06495-0
6. Wang Y, Zhang H, Yu J, et al. Psoralen-mediated regulation of osteogenic differentiation of periodontal ligament stem cells: involvement of the mTOR pathway. *Front Cell Develop Biol*. 2025;13:1634945. doi:10.3389/fcell.2025.1634945
7. Zhao C, Li K, Wu A. METTL1-mediated m7G modification regulates osteogenic differentiation of human periodontal ligament stem cells. *Clinics*. 2025;80:100813. doi:10.1016/j.clinsp.2025.100813
8. Zhang Q, Huang S, Wu J, et al. Spheroid culture of human periodontal ligament stem cells on agarose enhances stemness and osteogenic differentiation potential. *Am J Transl Res*. 2025;17(7):5257–5270. doi:10.62347/PPEI1766
9. Lowe B, Hardy JG, Walsh LJ. Optimizing Nanohydroxyapatite Nanocomposites for Bone Tissue Engineering. *ACS omega*. 2020;5(1):1–9. doi:10.1021/acsomega.9b02917
10. Fu Y, Cui S, Luo D, Liu Y. Novel Inorganic Nanomaterial-Based Therapy for Bone Tissue Regeneration. *Nanomaterials*. 2021;11(3):789. doi:10.3390/nano11030789
11. Takáč P, Michalková R, Čižmáriková M, Bedlovičová Z, Balážová Ľ, Takáčová G. The Role of Silver Nanoparticles in the Diagnosis and Treatment of Cancer: are There Any Perspectives for the Future? *Life*. 2023;13(2):466. doi:10.3390/life13020466
12. Chen F, Han J, Guo Z, et al. Antibacterial 3D-Printed Silver Nanoparticle/Poly Lactic-Co-Glycolic Acid (PLGA) Scaffolds for Bone Tissue Engineering. *Materials*. 2023;16(11):1.

13. Qing T, Mahmood M, Zheng Y, Biris AS, Shi L, Casciano DA. A genomic characterization of the influence of silver nanoparticles on bone differentiation in MC3T3-E1cells. *J Appl Toxicol*. 2018;38(2):172–179. doi:10.1002/jat.3528
14. Weng W, Li X, Nie W, et al. One-Step Preparation of an AgNP-nHA@RGO Three-Dimensional Porous Scaffold and Its Application in Infected Bone Defect Treatment. *Int J Nanomed*. 2020;15(null):5027–5042. doi:10.2147/IJN.S241859
15. Fahim M, Shahzaib A, Nishat N, Jahan A, Bhat TA, Inam A. Green synthesis of silver nanoparticles: a comprehensive review of methods, influencing factors, and applications. *JCIS Open*. 2024;16:100125. doi:10.1016/j.jciso.2024.100125
16. Rai M, Yadav A, Gade A. Silver nanoparticles as a new generation of antimicrobials. *Biotechnol Adv*. 2009;27(1):76–83. doi:10.1016/j.biotechadv.2008.09.002
17. Silambarasan T, Raja B. Diosmin, a bioflavonoid reverses alterations in blood pressure, nitric oxide, lipid peroxides and antioxidant status in DOCA-salt induced hypertensive rats. *Eur J Pharmacol*. 2012;679(1):81–89. doi:10.1016/j.ejphar.2011.12.040
18. Arafa E-SA, Elgendy NO, Elhemely MA, Abdelaleem EA, Mohamed WR. Diosmin mitigates dexamethasone-induced osteoporosis in vivo: role of Runx2, RANKL/OPG, and oxidative stress. *Biomed Pharmacother*. 2023;161:114461. doi:10.1016/j.biopha.2023.114461
19. Sahu N, Soni D, Chandrashekhar B, et al. Synthesis of silver nanoparticles using flavonoids: hesperidin, naringin and diosmin, and their antibacterial effects and cytotoxicity. *Int Nano Lett*. 2016;6(3):173–181. doi:10.1007/s40089-016-0184-9
20. Bogucka-Kocka A, Woźniak M, Feldo M, Kocki J, Szewczyk K. Diosmin – isolation Techniques, Determination in Plant Material and Pharmaceutical Formulations, and Clinical Use. *Nat Prod Commun*. 2013;8(4):1934578X1300800435. doi:10.1177/1934578X1300800435
21. Soheilikhah Z, Modarresi M, Karimi N, Movafeghi A. Qualitative and quantitative analysis of diosmin content of hyssop (Hyssopus officinalis) in response to salinity stress. *Heliyon*. 2021;7(10):e08228. doi:10.1016/j.heliyon.2021.e08228
22. Wassif RK, Elkheshen SA, Shamma RN, Amer MS, Elhelw R, El-Kayal M. Injectable systems of chitosan in situ forming composite gel incorporating linezolid-loaded biodegradable nanoparticles for long-term treatment of bone infections. *Drug Delivery Transl Res*. 2024;14(1):80–102. doi:10.1007/s13346-023-01384-x
23. Abdel-Gawad R, Osman R, Awad GAS, Mortada N. Wound healing potential of silver nanoparticles embedded in optimized bio-inspired hybridized chitosan soft and dry hydrogel. *Carbohydr Polym*. 2024;324:121526. doi:10.1016/j.carbpol.2023.121526
24. Kabeya JK, Ngombe NK, Mutwale PK, et al. Antimicrobial capping agents on silver nanoparticles made via green method using natural products from banana plant waste. *Artif Cells Nanomed Biotechnol*. 2025;53(1):29–42. doi:10.1080/21691401.2025.2462335
25. Ranoszek-Soliwoda K, Tomaszewska E, Socha E, et al. The role of tannic acid and sodium citrate in the synthesis of silver nanoparticles. *J Nanopart Res*. 2017;19(8):273. doi:10.1007/s11051-017-3973-9
26. Khan M, Karuppiah P, Alkhathlan HZ, et al. Green Synthesis of Silver Nanoparticles Using Juniperus procera Extract: their Characterization, and Biological Activity. *Crystals*. 2022;12(3):420. doi:10.3390/cryst12030420
27. David L, Moldovan B. Green Synthesis of Biogenic Silver Nanoparticles for Efficient Catalytic Removal of Harmful Organic Dyes. *Nanomaterials*. 2020;10(2):202. doi:10.3390/nano10020202
28. Saber SM, Gomaa SM, Elashiry MM, El-Banna A, Schäfer E. Comparative biological properties of resin-free and resin-based calcium silicate-based endodontic repair materials on human periodontal ligament stem cells. *Clin Oral Investigations*. 2023;27(11):6757–6768. doi:10.1007/s00784-023-05288-5
29. Sayed M, Mahmoud EM, Saber SM, Raafat SN, Gomaa SM, Naga SM. Effect of the injectable alginate/ nano-hydroxyapatite and the silica/ nano-hydroxyapatite composites on the stem cells: a comparative study. *J Non-Crystalline Solids*. 2023;610:122327. doi:10.1016/j.jnoncrysol.2023.122327
30. Shamel M, Raafat S, El Karim I, Saber S. Photobiomodulation and low-intensity pulsed ultrasound synergistically enhance dental mesenchymal stem cells viability, migration and differentiation: an invitro study. *Odontology*. 2024;112(4):1142–1156. doi:10.1007/s10266-024-00920-6
31. Nordin ML, Abdul Kadir A, Zakaria ZA, Abdullah R, Abdullah MNH. In vitro investigation of cytotoxic and antioxidative activities of Ardisia crispa against breast cancer cell lines, MCF-7 and MDA-MB-231. *BMC Complementary Alternat Med*. 2018;18(1):87. doi:10.1186/s12906-018-2153-5
32. Saleh A, Raafat SN, Sayed SA, Shamel M, Bahnasy SS, Shafei SFE. Simvastatin Enhances Stem Cell Osteogenesis and Reduces Peri-Implant Bone Loss: an In Vitro and a Randomized Clinical Study. *Pharmaceuticals*. 2026;19(3):368. doi:10.3390/ph19030368
33. Rodríguez-Lozano FJ, López-García S, García-Bernal D, et al. Cytocompatibility and bioactive properties of the new dual-curing resin-modified calcium silicate-based material for vital pulp therapy. *Clin Oral Investig*. 2021;25(8):5009–5024. doi:10.1007/s00784-021-03811-0
34. Krause U, Seckinger A, Gregory CA. Assays of osteogenic differentiation by cultured human mesenchymal stem cells. *Methods Mol Biol*. 2011;698:215–230.
35. Mazonde P, Khamanga SMM, Walker RB. Design, Optimization, Manufacture and Characterization of Efavirenz-Loaded Flaxseed Oil Nanoemulsions. *Pharmaceutics*. 2020;12(9):797. doi:10.3390/pharmaceutics12090797
36. Suresh N, Thomas NG, Mauramo M, Waltimo T, Sorsa T, Anil S. Phytonanoparticles as novel drug carriers for enhanced osteogenesis and osseointegration. *Discover Nano*. 2025;20(1):11. doi:10.1186/s11671-024-04164-9
37. Sabry GM, Sultan N, Abouelkhier MT, Farouk Soussa E. Osteogenic potential of silver nanoparticles in critical sized mandibular bone defects: an experimental study in white albino rats. *Odontology*. 2025;113(3):1062–1072. doi:10.1007/s10266-024-01049-2
38. Harun-Ur-Rashid M, Foyez T, Krishna SBN, Poda S, Imran AB. Recent advances of silver nanoparticle-based polymer nanocomposites for biomedical applications. *RSC Adv*. 2025;15(11):8480–8505. doi:10.1039/D4RA08220F
39. Akram M, Zafar SU, Salim M, Dar MS, Shakya S, Kabir Ud D. Synthesis of diester-bonded cationic gemini surfactant-coated silver nanoparticles: characterization, antibacterial activity, and interaction with bovine serum albumin. *J Dispers Sci Technol*. 2025;1–22. doi:10.1080/01932691.2025.2566249
40. Martínez-Cisterna D, Chen L, Bardehle L, et al. Chitosan-Coated Silver Nanocomposites: biosynthesis, Mechanical Properties, and Ag(+) Release in Liquid and Biofilm Forms. *Int J Mol Sci*. 2025;26(9):4130. doi:10.3390/ijms26094130
41. Edison TJI, Sethuraman MG. Instant green synthesis of silver nanoparticles using Terminalia chebula fruit extract and evaluation of their catalytic activity on reduction of methylene blue. *Process Biochem*. 2012;47(9):1351–1357. doi:10.1016/j.procbio.2012.04.025
42. Box GEP, Cox DR. An Analysis of Transformations. *J Royal Statistical Soc*. 1964;26(2):211–243. doi:10.1111/j.2517-6161.1964.tb00553.x
43. Piñeiro G, Perelman S, Guerschman JP, Paruelo JM. How to evaluate models: observed vs. predicted or predicted vs. observed? *Ecol Modell*. 2008;216(3):316–322. doi:10.1016/j.ecolmodel.2008.05.006

44. Na C, Osnovi RKN. Central composite design on the volume of laser metal deposited Ti6Al4V and Cu. *Materiali Tehnologije*. 2017;51(3):419–426. doi:10.17222/mit.2016.019
45. Thabet SS, Morsy M, Abdel-Gawad R. Dual statistical modeling using Box Behnken and d-optimal designs for optimization of indocyanine green conjugated silver nanoparticles and improvement of their associated photothermal therapy for application in wound healing. *J Pharmaceut Sci*. 2026;115(2):104077. doi:10.1016/j.xphs.2025.104077
46. Dagher W, Alassod A, Al Hinnawi MF, Alghoraibi I, Taher A, Alnhlaoui M. Characterization and antibacterial effect of green-synthesised silver nanoparticles using different extraction methods from Ziziphus spina-christi (Sidr) leaf extract collected from Syria. *RSC Adv*. 2025;15 (42):35642–35659. doi:10.1039/D5RA05214A
47. Eker F, Akdaşçi E, Duman H, Bechelany M, Karav S. Green Synthesis of Silver Nanoparticles Using Plant Extracts: a Comprehensive Review of Physicochemical Properties and Multifunctional Applications. *Int J Mol Sci*. 2025;26(13):6222. doi:10.3390/ijms26136222
48. Jiang XC, Chen WM, Chen CY, Xiong SX, Yu AB. Role of Temperature in the Growth of Silver Nanoparticles Through a Synergetic Reduction Approach. *Nanoscale Res Lett*. 2011;6(1):32. doi:10.1007/s11671-010-9780-1
49. Mohsen A, Abdel-Goad MA. Silver Nanoparticles from Nature: green Synthesis Methods and Applications-A Review. *J Adv Eng Trends*. 2025;44 (1):227–236. doi:10.21608/jaet.2024.319157.1334
50. Getachew AM, Bacha EG, Geleta WS. Statistical optimization of eco-friendly synthesized silver nanoparticles using Discopodium penninervium Hochst leaf extract for enhanced antimicrobial efficacy. *Sci Rep*. 2025;15(1):45017. doi:10.1038/s41598-025-29253-2
51. Abdelghany AM, Nagi Y, Oraby AH, Abdelaziz M, Abdelrazek EM. Green hydrothermal synthesis and optimization of gold/silver core-shell nanoparticles using thyme extract. *J Umm Al-Qura Univ Appl Sci*. 2025. doi:10.1007/s43994-025-00268-9
52. Serdar G, Gül Kılınç G, Mazlum Şen T. Green One-Pot Synthesis of Silver and Gold Nanoparticles Using Catechin Extracts: influence of Temperature and Antioxidant Activity Evaluation. *Plasmonics*. 2025;20(11):10691–10710. doi:10.1007/s11468-025-03083-4
53. Riaz M, Mutreja V, Sareen S, et al. Exceptional antibacterial and cytotoxic potency of monodisperse greener AgNPs prepared under optimized pH and temperature. *Sci Rep*. 2021;11(1):2866. doi:10.1038/s41598-021-82555-z
54. Izak-Nau E, Huk A, Reidy B, et al. Impact of storage conditions and storage time on silver nanoparticles' physicochemical properties and implications for their biological effects. *RSC Adv*. 2015;5(102):84172–84185. doi:10.1039/C5RA10187E
55. López-Lorente ÁI, Mizaikoff B. Recent advances on the characterization of nanoparticles using infrared spectroscopy. *TrAC Trends Anal Chem*. 2016;84:97–106. doi:10.1016/j.trac.2016.01.012
56. Link S, El-Sayed MA. Optical properties and ultrafast dynamics of metallic nanocrystals. *Annu Rev Phys Chem*. 2003;54(1):331–366. doi:10.1146/annurev.physchem.54.011002.103759
57. Taleb A, Petit C, Pileni MP. Optical properties of self-assembled 2D and 3D superlattices of silver nanoparticles. *J Phys Chem A*. 1998;102 (12):2214–2220. doi:10.1021/jp972807s
58. Ashraf JM, Ansari MA, Khan HM, Alzohairy MA, Choi I. Green synthesis of silver nanoparticles and characterization of their inhibitory effects on AGEs formation using biophysical techniques. *Sci Rep*. 2016;6(1):20414. doi:10.1038/srep20414
59. Loiseau A, Asila V, Boitel-Aullen G, Lam M, Salmain M, Boujday S. Silver-based plasmonic nanoparticles for and their use in biosensing. *Biosensors*. 2019;9(2):78. doi:10.3390/bios9020078
60. Wan Mat Khalir WKA, Shameli K, Jazayeri SD, Othman NA, Che Jusoh NW, Hassan NM. Biosynthesized silver nanoparticles by aqueous stem extract of Entada spiralis and screening of their biomedical activity. *Front Chem*. 2020;8:620. doi:10.3389/fchem.2020.00620
61. Srilatha D, Nasare M, Nagasandhya B, Prasad V, Diwan P. Development and validation of UV spectrophotometric method for simultaneous estimation of hesperidin and diosmin in the pharmaceutical dosage form. *Int Scholarly Res Notices*. 2013;2013(1):534830.
62. Car J, Krstulović N. Analytical model for determination of size-distribution of colloidal silver nanoparticles from surface plasmon resonance wavelength and dielectric functions. *Nanomaterials*. 2022;12(19):3474. doi:10.3390/nano12193474
63. Khan H, Gul A, Najam Z, Malik T. Biogenic silver nanoparticles optimization using Plackett–Burman design and its synergistic effect with cefotaxime against multidrug resistant clinical isolates. *Sci Rep*. 2025;15(1):18742. doi:10.1038/s41598-025-01524-y
64. Du L, Xu Q, Huang M, Xian L, Feng J-X. Synthesis of small silver nanoparticles under light radiation by fungus Penicillium oxalicum and its application for the catalytic reduction of methylene blue. *Mater Chem Phys*. 2015;160:40–47. doi:10.1016/j.matchemphys.2015.04.003
65. Fouad H, Hongjie L, Hosni D, et al. Controlling Aedes albopictus and Culex pipiens pallens using silver nanoparticles synthesized from aqueous extract of Cassia fistula fruit pulp and its mode of action. *Artif Cells Nanomed Biotechnol*. 2018;46(3):558–567. doi:10.1080/21691401.2017.1329739
66. Li Y, Xiao D, Li S, Chen Z, Liu S, Li J. Silver@quercetin Nanoparticles with Aggregation-Induced Emission for Bioimaging In Vitro and In Vivo. *Int J Mol Sci*. 2022;23(13):7413. doi:10.3390/ijms23137413
67. Faezi M, Motavalizadehkakhky A, Homayouni Tabrizi M, Dolatabadi S, Es-haghi A. Zein–sodium caseinate–diosmin nanoparticles as a promising anti-cancer agent with targeted efficacy against A2780 cell line. *Sci Rep*. 2025;15(1):8762. doi:10.1038/s41598-025-93772-1
68. Miranda RR, Sampaio I, Zucolotto V. Exploring silver nanoparticles for cancer therapy and diagnosis. *Colloids Surf B*. 2022;210:112254. doi:10.1016/j.colsurfb.2021.112254
69. Iravani S, Korbekandi H, Mirmohammadi SV, Zolfaghari B. Synthesis of silver nanoparticles: chemical, physical and biological methods. *Res Pharm Sci*. 2014;9(6):1.
70. Filippov SK, Khusnutdinov R, Murmiliuk A, et al. Dynamic light scattering and transmission electron microscopy in drug delivery: a roadmap for correct characterization of nanoparticles and interpretation of results. *Mater Horizons*. 2023;10(12):5354–5370. doi:10.1039/D3MH00717K
71. Khedr AIM, Farrag AFS, Nasr AM, et al. Comparative Estimation of the Cytotoxic Activity of Different Parts of Cynara scolymus L.: crude Extracts versus Green Synthesized Silver Nanoparticles with Apoptotic Investigation. *Pharmaceutics*. 2022;14(10):2185. doi:10.3390/pharmaceutics14102185
72. Xuan Y, Li L, Zhang C, Zhang M, Cao J, Zhang Z. The 3D-Printed Ordered Bredigite Scaffold Promotes Pro-Healing of Critical-Sized Bone Defects by Regulating Macrophage Polarization. *Int J Nanomed*. 2023;18:917–932. doi:10.2147/IJN.S393080
73. Xie C, Wang C, Huang W, et al. Recombinant human bone morphogenetic protein is a valid alternative to autologous bone graft for long bone non-unions: a systematic review and meta-analysis. *Surgeon*. 2023;21(4):e173–e182. doi:10.1016/j.surge.2022.11.004
74. Kungvarnchaikul I, Subbalekha K, Sindhavajiva PR, Suwanwela J. Deproteinized bovine bone and freeze-dried bone allograft in sinus floor augmentation: a randomized controlled trial. *Clin Implant Dentistry Related Res*. 2023;25(2):343–351. doi:10.1111/cid.13179

75. Moon YJ, Jeong S, Lee KB. Bone Morphogenetic Protein 2 Promotes Bone Formation in Bone Defects in Which Bone Remodeling Is Suppressed by Long-Term and High-Dose Zoledronic Acid. *Bioengineering*. 2023;10(1):86. doi:10.3390/bioengineering10010086
76. Sharma S, Porwal K, Kulkarni C, et al. Diosmin, a citrus fruit-derived phlebotonic bioflavonoid protects rats from chronic kidney disease-induced loss of bone mass and strength without deteriorating the renal function. *Food Funct*. 2022;13(4):2184–2199. doi:10.1039/D1FO03867B
77. Hu S, Huang Y, Chen Y, et al. Diosmetin reduces bone loss and osteoclastogenesis by regulating the expression of TRPV1 in osteoporosis rats. *Ann translat Med*. 2020;8(20):20. doi:10.21037/atm-20-6309
78. Bhattacharyya S, Pal S, Mohamed R, et al. A nutraceutical composition containing diosmin and hesperidin has osteogenic and anti-resorptive effects and expands the anabolic window of teriparatide. *Biomed Pharmacother*. 2019;118:109207. doi:10.1016/j.biopha.2019.109207
79. Sun X-C, Zhang Z-B, Wang H, Li J-H, Ma X, Xia H-F. Comparison of three surgical models of bone tissue defects in cleft palate in rabbits. *Int J Pediatric Otorhinolaryngol*. 2019;124:164–172. doi:10.1016/j.ijporl.2019.05.002
80. Xue N, Ding X, Huang R, et al. Bone Tissue Engineering in the Treatment of Bone Defects. *Pharmaceuticals*. 2022;15(7):879. doi:10.3390/ph15070879
81. Zhang R, Lee P, Lui VCH, et al. Silver nanoparticles promote osteogenesis of mesenchymal stem cells and improve bone fracture healing in osteogenesis mechanism mouse model. *Nanomed Nanotechnol Biol Med*. 2015;11(8):1949–1959. doi:10.1016/j.nano.2015.07.016
82. Kumar VB, Khajuria DK, Karasik D, Gedanken A. Silver and gold doped hydroxyapatite nanocomposites for enhanced bone regeneration. *Biomed Mater*. 2019;14(5):055002. doi:10.1088/1748-605X/ab28e4
83. Chandran SV, Vairamani M, Selvamurugan N. Osteostimulatory effect of biocomposite scaffold containing phytomolecule diosmin by Integrin/FAK/ERK signaling pathway in mouse mesenchymal stem cells. *Sci Rep*. 2019;9(1):11900. doi:10.1038/s41598-019-48429-1
84. Yu H, de Vos P, Ren Y. Overexpression of osteoprotegerin promotes preosteoblast differentiation to mature osteoblasts. *Angle Orthodontist*. 2011;81(1):100–106. doi:10.2319/050210-238.1
85. Mohamed SS, Zaki HF, Raafat SN. The Effect of Clopidogrel and Ticagrelor on Human Adipose Mesenchymal Stem Cell Osteogenic Differentiation Potential: in Vitro Comparative Study. *Adv Pharmacol Pharmaceutical Sci*. 2024;2024:2990670.
86. Chen H, Yan Y, Qi J, Deng L, Cui W. Sustained delivery of desferrioxamine via liposome carriers in hydrogel for combining angiogenesis and osteogenesis in bone defects reconstruction. *J Control Release*. 2017;259:e79.
87. Xie H, Wang P, Wu J. Effect of exposure of osteoblast-like cells to low-dose silver nanoparticles: uptake, retention and osteogenic activity. *Artif Cells Nanomed Biotechnol*. 2019;47(1):260–267. doi:10.1080/21691401.2018.1552594
88. Shalkami A, Hassan M, Bakr A. Anti-inflammatory, antioxidant and anti-apoptotic activity of diosmin in acetic acid-induced ulcerative colitis. *Hum Exp Toxicol*. 2017;37(1):78–86.